Tittle. Exosome-transmitted miR-769-5p confers cisplatin resistance and tumorigenesis in gastric cancer by targeting CASP9 and promoting the ubiquitination degradation of p53

Authors

Xinming Jing1*,Mengyan Xie1*, Kun Ding1*, Tingting Xu1, Yuan Fang1, Pei Ma#1, Yongqian Shu#1,2,3

1 Department of Oncology, The First Affiliated Hospital of Nanjing Medical University, China;

2 Jiangsu Key Lab of Cancer Biomarkers, Prevention and Treatment, Collaborative Innovation Center for Cancer Personalized Medicine, Nanjing Medical University, Nanjing, China.

Xinming Jing，Mengyan Xie, and Kun Ding contributed equally to this work.

Corresponding author: Yongqian Shu (email: shuyongqian2018@163.com); Pei Ma (email: mapei@njmu.edu.cn>)

Abstract

Cisplatin resistance is the main cause of poor clinical prognosis in patients with gastric cancer (GC). Yet, the exact mechanism of cisplatin resistance remains unclear. Recent studies have suggested that exocrine miRNAs found in the tumor microenvironment participates in tumor metastasis and drug resistance. In this study,

we discovered that cisplatin-resistant GC cells communicate with the tumor microenvironment by secreting microvesicles. The biologically active miR-769-5p can be integrated into exosomes and delivered to sensitive cells, thereby spreading cisplatin resistance. Mi769-5p was upregulated in GC tissues and enriched in the serum exosomes of cisplatin-resistant patients. Mechanistically, miR-769-5p promotes cisplatin resistance by targeting CASP9 so as to inhibit the downstream caspase pathway and promote the degradation of the apoptosis-related protein p53 through the ubiquitin-proteasome pathway. Targeting miR-769 with its antagonist to treat cisplatin-resistant GC cells can restore the cisplatin response, confirming that exosomal miR-769-5p can be a key regulator of cisplatin resistance in GC. Therefore, exosomal miR-769-5p derived from drug-resistant cells can be used as a potential therapeutic predictor of anti-tumor chemotherapy to enhance the effect of anti-cancer chemotherapy, which provides a new treatment option for GC.

Introduction

Gastric cancer (GC) is the leading cause of cancer-related death worldwide [1]. Cisplatin has been widely used for patients with advanced metastatic gastric cancer who are not eligible for surgery [2]. However, not all patients respond to cisplatin, which in turn leads to a poor prognosis [3]. Tumor resistance is a complex dynamic process of mutual influence between individuals and tumors. At the micro-level, it is the result of the mutual adaptation of the tumor microenvironment and tumor cells after chemotherapy [4]. The adaptive changes of tumor cells occur in an orderly

manner under the control of intricate signal networks and key molecules, in which the interaction of heredity, epigenetics, and post-translational protein modification has an important role.

MicroRNA (miRNA) is a non-coding RNA with a length of 18-22 nt, which regulates protein expression levels by blocking mRNA translation or inducing mRNA degradation [5]. It can modify the expression of target genes and regulate signal transduction and biological processes [6]. Changes in the expression of certain miRNAs in most tumors have been associated with tumor cell proliferation, angiogenesis, and drug resistance [7, 8].

The apoptotic signaling molecule CASP9 is one of the caspases, a family of proteins that regulates cell death [9, 10]. Anti-apoptosis is an important feature of malignant cells, which has been clearly related to tumor development and cancer resistance to treatment [11]. Targeting anti-apoptosis is considered to be a valuable strategy to improve susceptibility to apoptosis and the response to chemotherapy [12-14].

Another important molecule involved in apoptosis is p53, which can prevent abnormal cell proliferation and canceration and regulation of drug resistance [15, 16]. Evidence shows that up to 80% of cellular proteins are degraded by the ubiquitin-proteasome system (UPS), including p53. UPS is a specialized proteolytic system that controls protein degradation and has an important role in cellular protein homeostasis [17-21].

In this study, we hypothesized that CASP9 and p53 might be a potential target gene of miR-769-5p involved in miR-769-5p's inhibition of gastric cancer cell apoptosis and might induce cisplatin resistance.

Results

miR-769-5p is enriched in BGC823/DDP cell-derived exosomes

To isolate exosomes from BGC823 and BGC823/DDP cells, we purified the conditioned medium by using differential centrifugations. Under the transmission electron microscope, nanovesicles were seen as a round shape with bilayered membranes, and the diameter distribution of these nanovesicles ranged from 40nm to 150 nm for cryopreserved spheres (**Figure 1A**). NanoSight particle tracking analysis (NTA) of the size distributions and a number of exosomes revealed that the size of main vesicles secreted from BGC823 and BGC823/DDP cells was 82 nm and 89 nm, with concentrations of 1.13E+10 particles/ml and 7.29E+9 particles/ml, respectively (**Figure 1B**). By immunoblotting of lysates from purified nanovesicles and flow cytometry (FCM), the known exosomal markers TSG101, CD9, CD81and CD63 were detected (**Figure 1C** and **1D**). These results demonstrated that these nanovesicles isolated from BGC823 and BGC823/DDP express typical characteristics of exosomes.

Next, we compared the differences in miRNAs expressed in two cell-derived exosome populations by using sequencing analysis (**Figure 1E** and **F**). The level of miR-769-5p expressed in BGC823/DDP secreted exosomes (BD Exo) was 4.77 times that in BGC secreted exosomes (BC Exo). The expression of miR-769-5p in BD Exo

was 8.778±0.6923-fold greater than in BC Exo (**Figure 1G**). Moreover, using a TCGA database, we found that miR-769-5p has a promoting role in tumor (**Figure 1H**).

To detect the miR-769-5p expression levels in 79 pairs of clinical samples, we used the technique of RNA in situ hybridization (ISH). Our results revealed that miR-769-5p had markedly higher expression in tumor tissues compared with paracancerous tissues (**Figure 1I** and **1J**). The results indicated that the abundance of miR-769-5p in GC tissues was much higher than that in matched normal tissues, and the expression of miR-769-5p was correlated with advanced TNM stage, vascular invasion and poor prognosis. Additionally, we investigated the expression level of miR-769-5p in human GC serum samples. miR-769-5p expression level was significantly increased in exosomes of DDP-resistant patients' serum (n=19, as compared to respective parental DDP-sensitive patients' serum (n=41) (**Figure 1K**). These findings suggested that miR-769-5p may be involved in DDP sensitivity.

miR-769-5p is is required for GC cisplatin-resistance

Growing evidence indicates that exosomes released by cancer cells are enriched in miRNAs. Exosomal miRNAs can mediate phenotypical changes in the tumor microenvironment (TME) to promote tumor growth and therapy resistance. In this study, we hypothesized that miR-769-5p from BD Exo might participate in this process. We evaluated the effect of DDP on BGC823 cells in the presence of BD Exo and found that BD Exo significantly decreased the sensitivity of BGC823 cells to

cisplatin by CCK8 (**Figure 2C**). At a cisplatin concentration of 0.8 ug/ml, the survival of BGC823 cells increased after adding BD Exo compared with control. The half-maximal inhibitory concentration (IC50) of cisplatin was also increased. Additionally, the rates of BGC823 cells' apoptosis were reduced after being co-cultured with BD Exo for 24h (**Figure 2A** and **2B**). This data suggests that exosomes expression in resistant cells reduces IC50 and increases cell apoptosis of sensitive cells following cisplatin treatment.

A Transwell assay was used to examine whether the delivery of miR-769-5p occurs via exosomes. Briefly, we plated BGC823/DDP cells transfected with the Cy3-miR-769-5p mimics in the upper chamber and BGC823 cells in the lower chamber. The co-culture system was separated by 0.4 um pores, just allowing the transmission of micro particles such as exosomes but inhibiting direct contact between cells. After 24h, we found strong red fluorescence in BGC823 cells (**Figure 2D**). This phenomenon proved that miR-769-5p might be directly transferred from donor cells to recipient cells through exosomes. Furthermore, to visualize exosome transfer, we first incubated BGC823 cells and BD Exo in the presence of PKH26-labeled for 24 hours and evaluated the BD Exo uptake levels by measuring the red PKH26 signal in the BGC823 cell line. The confocal immunofluorescence microscopy detected a robust exosome signal in the cytoplasm of BGC823 cells after incubation of labeled BD Exo (**Figure 2E**), thus suggesting that BD Exo was successfully taken up BGC823 cells. **Figure 2J** shows that the co-incubation with BD Exo increased the expression of miR-769-5p. Importantly, intratumor injection of BD

Exo promoted the growth and induced the cisplatin resistance of GC cells compared to the same group injected with PBS (**Figure 5D-5G**). Taken together, we have reasons to believe that miR-769-5p might be transferred via exosomes from resistant GC cells to the neighboring sensitive GC cells, thereby spreading cisplatin resistance.

Exosome-mediated transfer of miR-769-5p targets CASP9 directly

To further explore the mechanism through which BD Exo and miR-769-5p induced cisplatin resistance, we investigated the target gene involved in mediating the effect of miR-769-5p on modulating apoptosis by miRanda, TargetScan, MiRWalk, and miRTarBase. We found that CASP9 was a target of miR769-5p in 3′-UTR area. Luciferase reporter assay further showed a significant reduction in luciferase activity when miR-769-5p was expressed in HEK293T cells as it did not affect the luciferase activity when the binding site was mutated (**Figure 2F** and **2I**). Furthermore, qRT-PCR and Western blotting showed that overexpression of miR-769-5p inhibited the expression of CASP9 in BGC823 cells, whereas inhibition of miR-769-5p reversed this process (**Figure 2G** and **2H**), thus suggesting that miR-769-5p can negatively regulate CASP9 at both the transcript and protein levels.

Next, we infected BGC823 cells with lentiviral vectors to construct cell lines stably expressing miR-769-5p inhibitor (BGC anti-769), negative control miRNA inhibitor (BGC anti-NC), or CASP9 overexpression (BGC CASP9). Then, we cocultured these cells directly with BD Exo (BGC anti-769 + BD Exo, BGC anti-NC + BD Exo and BGC CASP9 + BD Exo), BGC anti-NC incubated with the same

amount of PBS (BGC anti-NC+ PBS) were used as a negative control. **Figure 2J** (**SFig 1F**) shows that the co-incubation with BD Exo increased the expression of miR-769-5p in BGC anti-NC but had no effect on the expression of BGC anti-NC in BGC anti-769 cells. Compared with the control group BGC anti-NC+ PBS, the expression of CASP9 in BGC anti-NC + BD Exo was reduced. Nevertheless, when miR-769-5p was inhibited in BGC823, the impact above of reduction in CASP9 induced by BD Exo was offset (**Figure 2K** and **2L**, **SFig 1E** and **1G**). These results suggested that BD Exo can induce the upregulation of miR-769-5p and downregulation of CASP9 in recipient cells.

Transwell assay was used to further explore whether the delivery of miR-769-5p to recipient cells is dependent on exosomes**.** We plated BGC823/DDP cells with GW4869 in the upper chamber to prevent exocytosis, while BGC823 cells were seeded in the lower chamber. After 24 hours, we collected BGC823 cells and found that the expression of miR-769-5p in the cells (BGC+BD Exo GW4869) was significantly reduced compared with the control group cells treated with DMSO (BGC+BD Exo DMSO)(**Figure 2M**, **SFig 1I**). The CASP9 mRNA and protein expression were significantly increased (**Figure 2N** and **2O**, **SFig 1H** and **1J**). These results indicated that the delivery of miR-769-5p was dependent on exosomes.

In another experiment, we plated BGC823/DDP cells transfected with miR-769-5p inhibitor (BD 769 inhibitor) in the upper chamber and BGC823 cells in the lower one. We found that the co-cultured recipient cells CASP9 mRNA (**Figure**

2O, **SFig 1J**) and protein (**Figure 2P**, **SFig 1K**) levels were higher than the negative control. In addition, when BD cells in the upper chamber were co-transfected with anti-miR-769-5p and CASP9-siRNA (BD anti-769+siCASP9), and exosomes released from BD cells had no statistically significant effect on the mRNA and protein levels of CASP9 in the recipient cells. These results further confirmed that miR-769-5p was present in exosomes and that CASP9 was down-regulated by miR-769-5p.

Exosome-mediated transfer of miR-769-5p confers cisplatin resistance through downregulating CASP9 and subsequent evasion of apoptosis

Next, we determined that exosomal miR-769-5p confers cisplatin resistance in BGC823 cells by targeting CASP9. As shown in (**Figure 3A, SFig 2A**), BD Exo significantly enhanced the apoptosis of BC anti-NC cells by 4.483 ± 0.3153% induced by cisplatin (0.4 ug/ml, 24h), while no statistically significant difference was observed in BGC823 cells with miR-769-5p knockdown or CASP9 overexpression. Therefore, miR-769-5p knockdown or CASP9 overexpression could reverse the effect of BD Exo on the cisplatin resistance of BGC823 cells. Compared with BGC823/DDP cells treated with DMSO, after co-cultivation with BGC823/DDP cells treated with GW4869 (10 μM), the level of apoptosis of BGC823 cells induced by cisplatin was reduced by 4.470 ± 0.9988% (**Figure 3B**, **SFig 2B**). In addition, when they were co-cultured with miR-769-5p knockdown BGC823/DDP cells, the cisplatin resistance of BGC823 cells was reduced (**Figure 3C**, **SFig 2C**).

γ-H2AX is a sign of DNA double-strand breaks. After 24 h cisplatin treatment (0.8 ug/ml, 24h), the level of γ-H2AX nuclear foci in the control group remained high, but the nuclear foci in the BD Exo co-culture group significantly decreased by 36.77 ± 3.079% (**Figure 3D**, **SFig 3A**). However, there was no statistically significant difference observed in BGC823 cells with miR-769-5p knockdown or CASP9 overexpression. γ-H2AX expression levels in nuclear foci indicated that cisplatin induces more resistant cell lines after co-culturing with BD Exo. Similarly, after co-culturing with BGC823/DDP cells treated with GW4869 (10 μM), the level of γ-H2AX expression in nuclear foci of BGC823 cells induced by cisplatin was reduced by 37.47 ± 5.590% compared with BGC823/DDP cells treated with DMSO (**Figure 3E**, **SFig 3B**).

We then used a Transwell assay and co-cultured BGC823/DDP cells transfected with miR-769-5p inhibitor (BD anti-769) with BGC823 cells seeded in the lower chamber and found that γ-H2AX expression levels in nuclear foci of co-cultured recipient cells were higher than the negative control (**Figure 3F**, **SFig 3C**). Co-incubation of BGC823/DDP cells co-transfected with miR-769-5p inhibitor and CASP9-siRNA had no profound synergistic effect on γ-H2AX expression in BGC823 cells.

To further investigate the role of exosomal miR-769-5p cisplatin-induced apoptosis, we performed TUNEL analysis and found that it was consistent with the verification of flow cytometry assays (**Figure 3G**, **Figure 4A** and **B**, **SFig 3D-3F**).

The results showed that the exosomal miR-769-5p from cisplatin-resistant cells could accelerate cell apoptosis of cisplatin-sensitive cells. Western blots assay demonstrated that the protein levels of caspase-9 and cleaved caspase-3 in BGC anti-NC + BD Exo cells were reduced, yet there were no obvious differences in the BGC anti-769 + BD Exo and BGC CASP9 + BD Exo cells (**Figure 5A**, **SFig 4A**). Compared with BGC+BD Exo DMSO or BGC+BD anti-NC Exo cells, the caspase-9 and cleaved caspase-3 protein levels were increased in BGC823 cells co-cultured with BGC823/DDP cells treated with GW4869 or transfected with miR-769-5p inhibitor (**Figure 5B** and **5C**, **SFig 4B** and **4C**). Thus, these data suggested that the knockdown miR-769-5p could reverse the chemoresistance of gastric cancer cells to cisplatin.

Exosomal miR-769-5p promotes recipient cells proliferation and migration by downregulating CASP9

Next, we investigated whether exosomal miR-769-5p affects the biological processes of GC cells. BGC anti-NC cells treated with BD EXO showed increased colony formation, migration capacity compared to BGC anti-NC cells treated with PBS (**Figure 4C** and **4F**, **SFig 2D** and **2G**). Nevertheless, this alteration was reversed when BGC anti-769 or BGC CASP9 cells were co-cultured with BD Exo. In contrast, when BGC823 cells were co-cultured with BGC823/DDP treated with GW4869 or miR-769-5p knockdown, the colony formation, migration capacity of BGC823 cells decreased compared to those of the corresponding negative controls **(Figure 4D and 4E, 4G and 4H**, **SFig 2E** and **2F**, **SFig 2H** and **2I**). Our findings suggested that

exosomal miR-769-5p enhanced GC cell proliferation and migration by downregulating CASP9.

To sum up, the miR-769-5p was markedly upregulated in BGC823 cells treated with BD Exo, which suggested its potential role in cisplatin resistance and indicated the possibility of achieving the cisplatin resistance through the exosomal transfer of miR-769-5p by inhibiting CASP9 in GC cells.

miR-769-5p promotes ubiquitin-mediated p53 protein degradation in GC cells

It has been reported that the transcription factor P53 is essential in the complex molecular network regulating apoptosis, and the activation of tumor suppressor P53 is crucial for preventing abnormal cell proliferation and carcinogenesis. Many studies have shown that P53 is involved in regulating the generation of drug resistance. The main targets of P53 include P21, PUMA, BAX, and BID [22-24]. To further determine whether miR-769-5p is involved in GC cisplatin resistance and its molecular mechanism, we found that the targets of differentially expressed miRNAs were enriched in the p53 pathway based on the KEGG enrichment analysis of differently expressed miRNAs in exosomes (**Figure 6A**). Therefore, we hypothesized that miR-769-5p might affect the p53 pathway. To evaluate whether miR-769-5p is involved in p53-mediated apoptosis of gastric cancer cells, miR-769-5p expression in BGC823 and SGC7901 cells was overexpressed and knocked down using miR-769-5p mimics and inhibitors, respectively, after which the expression of p53 mRNA and protein were analyzed (**Figure 6B** and **6C**). Western blotting showed that

miR-769-5p silencing significantly enhanced the expression of p53 in GC cells, while overexpression of miR-769-5p had the opposite effects (**Figure 6C**). It indicated that miR-769-5p negatively regulates p53 protein expression and p53-mediated apoptosis in gastric cancer cells. However, qRT-PCR showed that the transcription level of p53 was not affected by miR-769-5p in gastric cancer cells, indicating that the p53 protein in gastric cancer cells may be degraded by ubiquitination (**Figure 6B**). As a result, we transfected miR-769-5p inhibitors into GC cells, and twenty-four hours later, the cells were treated with 20 μg/ml cycloheximide (CHX) changes with treatment time (0h, 1h, 4h). The cell lysates were then collected within a specified time period and analyzed by Western blot. Higher expression of p53 protein was detected in the cells treated with CHX compared with negative controls (**Figure 6E**, **SFig 4D**). We also treated the cells with MG-132, a specific inhibitor of a ubiquitin-binding protein, and found that higher expression of p53 protein was detected in the cells treated with MG-132 (10um) for 6h (**Figure 6F**, **SFig 4E**), indicating that p53 protein degradation depends on the ubiquitination.

According to ubibrowser, we characterized the p53-specific E3 ubiquitin ligases to determine the mechanism of miR-769-5p mediated p53 ubiquitination in GC cells. We selected the top five p53 E3 ubiquitin ligases to be silenced by sequence-specific small interfering RNA (siRNA) in HEK-293T. Detection of p53 protein showed that when NEDD4L expression is knocked down by sequence-specific siRNA, p53 levels increase (**Figure 6G**). NEDD4L is the key E3 ubiquitin ligase for p53 ubiquitination

in GC cells [25-27]. However, the negative control of NEDD4L-siRNA did not affect p53 expression.

Co-immunoprecipitation (Co-IP) and Western blotting were used to detect the interaction between NEDD4L and p53 in gastric cancer cells (**Figure 6H** and **6J, SFig 4F** and **SFig 4H**). The NEDD4L overexpression plasmid and His-Ub plasmid were co-transfected in BGC, and the ubiquitination level of p53 was detected by immunoprecipitation and Western blotting. NEDD4L overexpression promoted the ubiquitination of p53 (**Figure 6I**, **SFig 4G**), indicating that NEDD4L mediates the ubiquitination modification. In order to further evaluate the effect of miR-769-5p on the expression of NEDD4L, we inhibited and overexpressed miR-769-5p in gastric cancer cell lines to detect the expression of NEDD4L and p53 protein levels (**Figure 6K**, **SFig 4I**). Compared with the negative control group, knockdown of miR-769-5p significantly reduced the expression of NEDD4L and increased the expression level of p53, while overexpression of miR-769-5p showed the opposite result. Western blot also demonstrated that NEDD4L silencing caused p53 protein accumulation in miR-769-5p-silenced cancerous cells. This indicated that the inhibition of miR-769-5p could inhibit the expression of E3 ubiquitinated ligase NEDD4L, increasing the level of substrate p53. These data suggested that miR-769-5p could promote NEDD4L's expression, leading to its participation in the p53 ubiquitination degradation process.

E3 ubiquitination ligase RNF20 participates in miR-769-5p mediated p53 protein ubiquitination in GC cells

According to the miRNAs target gene prediction, we found that NEDD4L was not the target gene of miR-769-5p. So, it was unclear how miR-769-5p regulates and inhibits the expression of NEDD4L. Based on the miRNA target gene prediction website and UbiBrowser website, we found that E3 ubiquitin ligase RNF20 might be the target gene of miR-769-5p (**Figure 6L**, **6M** and **6N**). To characterize the interaction between miR-769-5p and RNF20, a dual-luciferase reporter assay was conducted in HEK293T cells. The results revealed that miR-769-5p significantly decreased the activity of the reporter luciferase that was fused with the wild-type RNF20 3-untranslated region (UTR) compared with the controls (**Figure 6O**). This observation suggested a direct interaction between miR-769-5p and RNF20 mRNA. Reports showed that a low RNF20 level was correlated with shortened overall survival and disease-free survival, indicating poor prognosis in cancers [28, 29].

Additionally, we discovered that RNF20 and NEDD4L interacted in GC cells. We transfected silenced and overexpressed RNF144B and negative control plasmids in BGC823 and tested the effect of RNF20 on apoptosis by TUNEL experiment (**Figure 7A** and **7D**, **SFig 5A** and **5C**) and immunofluorescence detection of γ-H2AX expression level (**Figure 7B** and **7E**, **SFig 5B** and **5D**). TUNEL results showed that compared with the negative control group, overexpression of RNF20 significantly promoted the apoptosis of gastric cancer cells while inhibition of RNF20 inhibited cell apoptosis. The results of immunofluorescence detection of γ-H2AX expression level were consistent with the results of the TUNEL experiment. Moreover, Western blot showed that the overexpression of RNF144B resulted in increased cleaved

caspase 3 and related to activated apoptosis (**Figure 7C** and **7F**, **SFig 6A** and **6B**). The activation of apoptosis by RNF20 overexpression was further confirmed by flow cytometry assay (**Figure 7H**). The above results indicate that RNF20, as a target gene of miR-769-5p, can participate in cell apoptosis.

RNF20 can be used as a target gene of miR-769-5p to participate in cell apoptosis. Thus, we further determined how RNF20 conveys apoptotic signals in p53-mediated cell apoptosis. The gene expression of RNF20 was silenced or overexpressed in GC cells, followed by RNF20 and p53 protein detection. RNF20 overexpression markedly suppressed NEDD4L expression and simultaneously induced p53 expression in gastric cancer cells (**Figure 7G**, **SFig 6C**), while silencing the RNF20 gene had the opposite effect on NEDD4L and p53 expression in gastric cancer cells. Furthermore, we overexpressed the RNF20 plasmid in GC cells and performed Co-IP with anti-RNF20 to identify proteins that interacted with RNF20. Our results indicated that RNF20 was bound to NEDD4L (**Figure 7I**, **SFig 6D**), thus suggesting that RNF20 participates in p53-mediated gastric cancer cell apoptosis by regulating NEDD4L expression.

To clarify whether NEDD4L could be ubiquitinated by RNF20 (**Figure 7Q** and **7R**, **SFig 6E** and **6F**), the His-Ub and RNF20 were co-expressed in GC cells, and anti-NEDD4L were used to pull down modified proteins. The presence of polyubiquitinated NEDD4L was observed as a smeared band because of the heterogeneous modification of this protein. At the same time, we stained the

polyubiquitinated NEDD4L in the flag-Ub immunoprecipitants to confirm that the ubiquitination modification of NEDD4L was mediated by RNF20 and found that RNF20 overexpression further enhanced the polyubiquitinated NEDD4L compared with the control. These findings revealed that RNF20 was an E3 ligase for NEDD4L and that RNF20 polyubiquitinated NEDD4L for degradation.

Exosomal miR-769-5p induces cisplatin resistance and promotes the tumorigenesis of GC *in vivo*

Given the observed effects of exosomal miR-769-5p on GC cells *in vitro*, we subsequently confirmed the aforementioned results *in vivo*. To determine whether miR-769-5p sensitizes GC cells to chemotherapeutic agents *in vivo*, anti-miR-769-5p transfected BGC823/DDP cells were subcutaneously implanted into nude mice and then treated with cisplatin (DDP, 4mg/kg). Our data indicated that miR-769-5p knockdown significantly decreased cisplatin resistance in BGC823/DDP xenografts (**Figure 8A-8E**). Levels of exosomal miR-769-5p were approximate two folds lower in the serum than that of the negative control group, and the expression levels of CASP9, p53, and cleaved caspase3 were decreased when the level of miR-769-5p increased in the subcutaneous tumor tissues of mice (**Figure 8N**). These data support our findings that knockdown miR-769-5p ameliorates cisplatin-resistant GC *in vitro* and *in vivo*.

In addition, we subcutaneously injected the stably transfected BGC 823 NC and BGC823 769 cells into nude mice and found that the tumors of BGC823 769 grew

357 faster than those of BGC823 NC. After cisplatin treatment, the tumor volume of the
358 BGC823 769 group was significantly higher compared to BGC 823 NC group
359 (**Figure 8F-8J**). These results indicated that miR-769-5p could promote growth and
360 induce the cisplatin resistance of BGC823 cells *in vivo*. Collectively, miR-769-5p
361 expression was indispensable for cisplatin resistance in GC cells.

362 **Discussion**

363 Chemotherapy is the most important treatment for patients who cannot
364 undergo surgery or those with advanced metastatic gastric cancer [30]. Yet,
365 multidrug resistance, which has been associated with a poor prognosis, remains a
366 big challenge when treating cancer patients [31]. For example, cisplatin resistance
367 presents a big obstacle in treating patients with advanced gastric cancer.

368 miRNAs can be encapsulated in exosomes to avoid degradation. Exosomal
369 miRNA can be transported to recipient cells and change their phenotype through
370 changes in gene expression [32-34]. For example, drug-resistant cancer cells may
371 release exosomal miRNAs into the microenvironment, causing the recipient cells to
372 develop drug resistance [35-37]. This ability of exosomes shed from tumor-resistant
373 cells to transfer drug-resistant phenotypes to drug-sensitive cells is considered an
374 important mechanism of drug resistance that is mainly spread mainly by drug efflux
375 pump and miRNAs' transfer. Numerous studies have reported that exosomes have
376 an important role in invasive tumor progress and chemotherapy resistance.

377 Our results showed that miR-769-5p in exosomes derived from

cisplatin-resistant cells could confer drug-resistant phenotypes on recipient cells and alter their gene expression and apoptosis. This is because when BGC823 cells treated with exosomes respond to cisplatin, the survival time increases. We also found that BD Exo inhibits the effect of cisplatin in BGC823 cells by transferring miR-769-5p. However, transfection of anti-miR-769 into BD cells partially blocked the effect of BD exo on cisplatin. **Figure 8k** summarizes the mechanism through which drug-resistant cells transfer mir-769-5p-loaded exosomes to sensitive cells and modulated cisplatin resistance. Mechanistically, exosomal miR-769-5p inhibits cell apoptosis by targeting the downstream caspase pathway of CASP9 inactivation and enhancing the drug resistance of recipient cells to cisplatin **(Fig. 8K)**.

The activation of the tumor suppressor p53 is essential to prevent abnormal cell proliferation and canceration. Many studies have shown that p53 is involved in the regulation of drug resistance. For example, phosphorylation of p53 serine 15 (Ser15) and serine 20 (Ser20) has been identified as essential in cisplatin resistance [38, 39]. As a key cellular protein regulator, ubiquitination can cause protein degradation. In the process of protein ubiquitination, E3 ubiquitin ligase determines substrate specificity and substrate selection. In addition, the mechanism of ubiquitin-mediated p53 protein degradation has been extensively studied [40, 41]. For example, mdm2-dependent p53 polyubiquitination and degradation can regulate cell proliferation, DNA damage-induced apoptosis, and tumorigenesis by inhibiting p53 [42, 43]. However, the role of miRNA in the regulation of p53 protein ubiquitination remains unclear.

Looking for the target genes of miR-769-5p, we found that miR-769-5p promotes the degradation of p53 and inhibits apoptosis through the ubiquitin-proteasome pathway, thus promoting the resistance of gastric cancer cells to cisplatin. Our study revealed a new mechanism of p53 protein ubiquitination mediated by miR-769-5p in cisplatin resistance. As an important apoptosis-related protein, miR-769-5p participates in the apoptosis of gastric cancer cells through the RNF20-NEDD4L-p53 pathway in the process of induced apoptosis, and miR-769-5p can directly inhibit the expression of RNF20. Previous studies have shown that HBRE1 /RNF20 is the E3 ubiquitin ligase of hiprotein H2B, and the deletion of RNF20 as a tumor suppressor can lead to the overall decrease of H2Bub level[44, 45]. Our results showed that RNF20 had a critical role in p53 protein ubiquitination in gastric cancer cells, mediating the direct degradation of p53 protein by E3 ubiquitin ligase NEDD4L, thus revealing a novel miRNA-mediated p53 protein ubiquitination pathway (**Figure 8K**).

Cancer is a complex genetic disease. Chemotherapy and radiation therapy have always been the core treatment options for cancer. However, these treatments have adverse side effects. Due to malignant tumors being highly heterogeneous in their occurrence and development, this study proved that miR-769-5p, which is highly expressed in drug-resistant gastric cancer cells, can be transferred to recipient cells sensitive to cisplatin via exosomes. The specific induction of gastric cancer cell apoptosis and cisplatin resistance indicates that inhibiting miR-769-5p may represent a potential therapeutic intervention strategy for the treatment of refractory gastric

cancer.

Materials and methods

All the materials and methods, and abbreviations are included in **Supplementary Materials and Methods**.

Supplementary Materials and Methods

Patient tissue and blood samples

Samples for cancer patients, including tissue and plasma specimens, were collected from the First Affiliated Hospital of Nanjing Medical University. Blood samples (serum) from 19 cisplatin-resistant patients and 41 cisplatin-sensitive patients were collected and stored at −80 °C. Other samples of 150 cases (75 pairs of GC tumor and normal tissuess) were embedded with 75 paraffin and analyzed by tissue microarray. Clinicopathological features, including age, sex, tumor site, tumor size, differentiation grade, Lauren classification, TNM stage (American Joint Committee on Cancer classification, AJCC), and lymphatic invasion, were also collected and analyzed (Table 1). This study was approved by the Ethics Committee of the First Affiliated Hospital of Nanjing Medical University. All patients signed an informed consent.

Cell culture and treatment

The HEK-293T cell line was purchased from Type Culture Collection of the Chinese Academy of Sciences (Shanghai, China). Gastric cancer BGC823, SGC7901 cell lines,

cisplatin-resistant BGC823/ DDP, and SGC7901/DDP cells were a kind gift from Professor Jianwei Zhou (School of Public Health, Nanjing Medical University). All cell lines were cultured in RPMI 1640 media (Gibco, Carlsbad, CA, USA) containing 10% fetal bovine serum (FBS) (ScienCell, CA, USA) and supplemented with 100 μg/ml streptomycin, 100 U/ml penicillin in a humidified atmosphere containing 5% CO2 at 37 °C. BGC823/ DDP and SGC7901/ DDP cells were cultured in a medium maintained with 0.5 μg/ml cisplatin (First Affiliated Hospital of Nanjing Medical University). Before the experiments, cell were cultured in a drug-free medium for at least 7 days. Cycloheximide (CHX)(Sigma-Aldrich, MO, USA) and MG132 (Selleck Chemicals, USA) were used at the indicated concentrations.

Exosome isolation and characterization

Cell culture supernatant was collected after being washed with PBS and incubated with freshly prepared complete medium containing exosome-free FBS for 48h. Exosomes were isolated from the conditioned medium by differential centrifugation. Conditioned medium was centrifuged at 300 g for 10 min and then at 2,000 g for 20 min at 4 ° C. The supernatant was then passed through a 0.22- μ m filter (Millipore, Burlington, MA, USA) to remove shedding vesicles and other vesicles larger in size. Finally, the supernatant was centrifuged at 110,000 × g for 70 min. Pelleted exosomes were resuspended in PBS and collected by ultracentrifugation again at 100,000 g for 90 min (all steps were performed at 4 ° C). Exosomes were collected from the pellet and resuspended in 100 μ L of PBS and subjected to several

experiments. The fractionation and purification of exosomes from conditioned media (CMs) and blood serum were collected by ultracentrifugation (Beckman Coulter) and ExoQuick Exosome Precipitation Solution (SBI, CA, USA) respectively. Exosomes were then identified by Transmission Electron Microscope (TEM) (Philips TECNAI 20, Netherland), and their particle morphology and size were analyzed. The concentration and number of exosomes were detected by nanoparticle tracking analysis (NTA). Exosome protein markers were identified by Western blot assay and flow cytometry analysis (FACS Calibur, BD Biosciences, USA) .

PKH26 Staining for Exosomes

The isolated exosomes were labeled with PKH26 Red Fluorescent Cell Linker Kits (Sigma). Exosomes were first resuspended in 100 μL Diluent C. A dye solution (4 × 10−6 M) was prepared by adding 0.4 μL PKH26 ethanolic dye solution to 100 μL Diluent C. The 100 μL exosome suspension was then mixed with the 100 μL dye solution by pipetting. After incubating the cell and dye suspension for 5 min with periodic mixing, the staining was stopped by adding 200 μL serum and incubating for 1 min. The stained exosomes were finally washed twice with 1× PBS, and they were resuspended in a fresh sterile conical polypropylene tube.

Lentiviral, plasmid, and microRNA mimics/inhibitors package and cell transfection

The lentivirus encoding miR-769-5p overexpression or knockdown and negative

control (769, NC, anti-769, anti-NC) were designed and produced by GENECHEM (Shanghai, China). The lentivirus were added to BGC823 BGC823/DDP, SGC7901 and SGC7901/DDP cells respectively and stable cell lines were obtained by selection with puromycin (Sigma-Aldrich, MO, USA). The infection efficiency was confirmed by fluorescence microscopy and real-time quantitative RT-PCR (qRT-PCR). pcDNA3.1 vector containing CASP9-wt, CASP9-mut, RNF20-wt or RNF20-mut, and a control vector were purchased from GENECHEM (Shanghai, China). miR-769-5p mimics, inhibitor and control, Cy3-miR-769-5p mimics and control were produced by GenePharma (Shanghai, China). Plasmids and miRNA mimics or inhibitors were transfected into cells with Lipofectamine 3000 (Invitrogen) according to the manufacturer's instructions. The siRNAs and controls were designed and synthesized by RiboBio (Guangzhou, China). The siRNAs were transfected into the cells by DharmaFECT4 (Dharmacon, IL, USA); all sequences are listed in **Additional file 2 Table S1**.

RNA extraction and quantitative RT-PCR

Total cellular and exosomal RNA was extracted from exosomes, co-cultured cells or GC cells, and frozen xenograft tumor tissues using TRIzol reagent (Invitrogen, CA, USA). Isolated RNA was used for the reverse transcription reaction with HiScript Q RT SuperMix for qPCR (Vazyme, Jiangsu, China). Quantitative RT-PCR was carried out with SYBR Green PCR Master Mix (Vazyme) using an ABI Prism 7900 Sequence detection system (Applied Biosystems, Canada). The relative expression of

503 miR-769 was normalized to U6 levels, and CASP9, RNF20, p53 mRNA expression
504 were normalized to GAPDH by qPCR using Power SYBR Green (Takara, Dalian,
505 China). Data were calculated by the2 (−ΔΔCT) method. The related primers are
506 synthesized by Ribobio (Guangzhou, China) and listed in **Additional file 2: Table**
507 **S2**.

508 **Dual-luciferase reporter assays**

509 293T cells (3 × 104 cells per well) were seeded onto 24-well plates 1 day before
510 transfection and were co-transfected by Lipofectamine™ 3000 (Invitrogen, USA)
511 with luciferase reporter (200 ng per well) using pmiR-REPORT™ luciferase vectors
512 (pmirGLO) containing wild-type or mutant 3`-UTR of CASP9 and RNF20 and
513 miR-769-5p mimics or miR-769-5p mimic-NC to examine the miRNA binding ability.
514 The cells were washed and lysed with the passive lysis buffer from the
515 Dual-Luciferase Reporter Assay System (Promega Corp). About 24 h later, a
516 Dual-Luciferase Reporter Assay kit (Promega, USA) was used to measure the
517 luciferase and renilla activity of these samples according to the manufacturer's
518 instructions. Relative luciferase activity was first normalized with Renilla luciferase
519 activity and then compared with those of the respective control. Wild-type and
520 mutated CASP9 or RNF20 3′ UTRs were synthesized and inserted into the
521 p-MIR-REPORT plasmid by Genechem, Shanghai, China.

522 **Colony formation assay**

523 GC cells (500 cells/well in six-well) were performed to detect the proliferation

524 capacity. After incubation at 37 °C, 5% CO2 for two weeks, the plates were washed
525 with PBS, fixed with 4% paraformaldehyde, stained with 0.1% crystal violet, washed
526 three times with water, and analyzed. The assay was repeated three times in duplicate,
527 and the numbers of colony formation counted.

528 **Cell viability assay**

529 Cells (1 × 104/well) were seeded in 96-well plates and treated with cisplatin from 0.2
530 to 6.4 μg/ml for 24 h. A CCK-8 assay was performed to detect cells viability using a
531 Cell Counting Kit 8 (Dojindo, Japan) and a OD450 nm (Synergy4; BioTek, Winooski,
532 VT, USA). Based on protocols of CCK-8 kits cells were seeded, cultured for 24 h,
533 and further cultured in 100 μL medium with 10 μL CCK-8 reagent. Absorbance at
534 450 nm was determined using a Multiscan FC plate reader (Thermo Fisher).

535 **Cell Migration Assay**

536 The migratory capacity of GCs was tested by using a Transwell Boyden Chamber
537 (6.5 mm, Costar) with polycarbonate membranes (8-μm pore size) on the bottom of
538 the upper compartment. A total of 2 × 104 cells was suspended in serum-free media.
539 Meanwhile, the lower chambers were loaded with 0.5 mL RPMI1640 containing 5%
540 FBS, and the plates containing Transwell inserts were incubated. After incubation at
541 37 °C, 5% CO2 for 12 h, the upper chamber was cleaned with a cotton swab, and the
542 lower chamber was washed with PBS. The cells that penetrated through the
543 membrane were fixed with 90% ethanol for 15 min at room temperature, stained with
544 0.1% crystal violet solution, washed three times with water, and imaged by Inversion

Microscope (Zeiss, Germany). The assay was repeated three times in duplicate. We obtained images of migrated cells by using a photomicroscope, and we quantified cell migration by blind counting with five fields per chamber.

Apoptosis assay

The flow cytometry analysis was performed by Annexin V-APC/PI Apoptosis Detection Kit (Vazyme, Jiangsu, China) according to the manufacturer's instructions. The cells were analyzed with a BD FACS Calibur flow cytometer using CellQuest Pro software (FACS Calibur, BD Biosciences, USA).

TUNEL assay

GC cells were fixed with paraformaldehyde for 30 min on ice. Then, terminal deoxynucleotidyl transferase dUTP nick end labeling (TUNEL) kit was used according to the manufacturer's instructions (TUNEL BrightGreen Apoptosis Detection Kit, Vazyme, Jiangsu, China) and DAPI (4′,6-diamidino-2-phenylindole) was used for nuclear staining. TUNEL-positive areas were quantified under an Olympus FSX100 microscope (Olympus, Tokyo, Japan).

Fluorescence assay

4′,6-diamidino-2-phenylindole (DAPI) (Invitrogen, USA) was used for cell nuclear staining. Rhodamine-conjugated secondary antibody (Cell Signaling Technology, USA) for γ-H2AX (1:250, Abcam, ab81299) protein and DAPI for nuclear staining. The slides were visualized for immunofluorescence with a laser scanning microscope

(Zeiss, Germany).

Western blot, immunohistochemistry (IHC), and immunoprecipitation (IP) assay

Cell or tissue samples were lysed by RIPA buffer mixed with protease and phosphatase inhibitor cocktails. Serum proteins were extracted with Serum Protein Extraction Kit (Qcheng Bio, China). The proteins were then separated by 10% SDS-PAGE and transferred onto PVDF membranes. Western blot assays were performed according to previously reported data [1]

The immune-complexes were detected with ECL Western Blotting Substrate (Thermo Fisher) and visualized with BIO-RAD (BIO-RAD Gel Doc XR+, USA). Immunohistochemistry and immunoprecipitation were done as previously reported [2]. Positive cells were counted in five random fields per slide. Primary antibodies and appropriate secondary antibodies used for the experiments are listed: TSG101 (1:1000, Abcam, ab125011), Calnexin (1:1000, Abcam, ab92573), CD81 (1:1000, Proteintech, 66866-1-Ig), CD63 (1:1000, Abcam, ab134045), γ -H2AX (1:250, Abcam, ab81299), caspase-9 (1:1000, CST, # 9504S), caspase-3 (1:1000, CST, # 9662), cleaved caspase-3 (1:1000, CST, # 9661), BAX (1:10000, Proteintech, 50599-2-Ig), Bcl-2 (1:1000, CST, #3498), p53 (1:5000, Proteintech, 10442-1-AP), NEDD4L (1:5000, Proteintech, 13690-1-AP), RNF20(1:1000, Proteintech, 21625-1-AP), Ubiquitin(1:1000, CST, # 3936S), β-actin (1:1000, Beyotime, AF0003), GAPDH (1:1000, Beyotime, AF0006). Incubation with the goat anti-rabbit secondary antibody (1:1000, Beyotime, A0208) or the goat anti-mouse secondary antibody

(1:1000, Beyotime, A0216).

RNA in situ hybridization (ISH)

BaseScope™ Reagent Kit v2-RED (Advanced Cell Diagnostics, CA, USA) was used for ISH following the user manual. RNA in situ hybridization (ISH) was performed according to previously reported data . Standard RNAScope protocols were used according to manufacturer's instructions and were performed according to previously reported data [3]. The following probes were used: miRNAscope Probe - SR-hsa-miR-769-5p-S1 (ACD; 1029501-S1), miRNAscope Positive Control Probe - SR-RNU6-S1 (ACD; 727871-S1), miRNAscope Negative Control Probe - SR-Scramble-S (ACD; 727881-S1).

A nude mouse model

4-week-old (BALB/c) were obtained from Model Animal Research Center Of Nanjing University, China. All the animals were housed in an environment with a temperature of 22 ± 1 ºC, relative humidity of 50 ± 1%, and a light/dark cycle of 12/12 hr and had access to water and food *at libitum*. All animal studies (including the mice euthanasia procedure) were done in compliance with the regulations and guidelines of Nanjing Medical University institutional animal care and conducted according to the AAALAC and the IACUC guidelines (IACUC-1902006)

a. Forty 4-week-old (BALB/c) male nude mice were randomly divided into two groups (20 mice in each group): BGC823+PBS and BGC823+BD EXO group.

606 Briefly, 5 × 10^6 BGC823 cells (100μL) were subcutaneously injected into the right
607 flank of nude mice. When the average volume of nude mice reached approx. 50mm^3,
608 one group was intratumorally injected with BGC/DDP EXO (200ug/100μL cells per
609 mouse) once every two days. When the tumor volume was 150-200mm^3, each group
610 were divided into two groups (10 mice in each group): BGC823+PBS+PBS,
611 BGC823+PBS+DDP, BGC823+BD EXO+PBS and BGC823+BD EXO+DDP group,
612 one group (BGC823+PBS+DDP, BGC823+BD EXO+DDP) was intraperitoneally
613 injected with DDP (4mg/kg per mouse) every three days, and the other group
614 (BGC823+PBS+PBS, BGC823+BD EXO+PBS) was injected with normal saline as
615 the control group.

616 b. Forty 4-week-old (BALB/c) male nude mice were randomly divided into two
617 groups (20 mice in each group): BGC NC and BGC 769. BGC823 cells with stable
618 overexpression of miR-769-5p (BGC 769) and control cells (BGC NC) (5 ×
619 10^6/100μL cells per mouse) were subcutaneously injected into the right flank of nude
620 mice. When the average volume of nude mice was about 150-200mm^3, each group
621 was divided into two groups: BGC NC+PBS, BGC 769+PBS, BGC NC+DDP and
622 BGC 769+DDP. One group (BGC/DDP anti769+DDP, BGC/DDP anti-NC+DDP)
623 was intraperitoneally injected with DDP according to the standard of 4mg/kg every
624 three days, and the other group (BGC NC+PBS, BGC 769+PBS) was
625 intraperitoneally injected with normal saline as control.

626 c. Forty 4-week-old (BALB/c) male nude mice were randomly divided into two

groups: BGC/DDPanti-769 and BGC/DDP anti-NC, with 20 mice in each group. BGC/DDP cells and control cells with stable knockdown expression of miR-769-5p (5×10^6/100 μ L cells per mouse) were injected subcutaneously into the right flank of nude mice. When the average volume of nude mice was about 150-200mm^3, each group was divided into two groups on average: BGC/DDPanti-769+PBS, BGC/DDP anti-NC+PBS, BGC/DDP anti769+DDP and BGC/DDP anti-NC+DDP. One group (BGC/DDP anti769+DDP, BGC/DDP anti-NC+DDP) was intraperitoneally injected with DDP according to the standard of 4mg/kg every three days, and the other group (BGC/DDPanti-769+PBS, BGC/DDP anti-NC+PBS) was intraperitoneally injected with normal saline as control.

Three weeks later, mice were sacrificed, and tumor tissues were prepared for histological examination: H&E staining, Western blot, and IHC assays. Tumor volume was measured using the following formula: $Tumor\ volume\ (mm^3) = 0.5 \times width^2 \times length$.

Statistical analysis

Statistical data were expressed as mean ± SD. One-way analysis of variance was used for three groups and more than three groups. All of the statistical analyses were assessed by software SPSS version 13.0 (SPSS, Chicago, IL, USA)and GraphPad Prism (GraphPad Software, Inc., SanDiego, CA, USA) software, comparisons among groups were done by the independent sample two-sided Student t-test. The ANOVA was performed to evaluate the statistical differences among groups. P- value of 0.05

or less was considered as statistical significance.

References:

1. Zhou, J., Ye, J., Zhao, X., Li, A., and Zhou, J. (2008). JWA is required for arsenic trioxide induced apoptosis in HeLa and MCF-7 cells via reactive oxygen species and mitochondria linked signal pathway. *Toxicol Appl Pharmacol* 230: 33-40.

2. Qiu, D., et al. (2018). RNF185 modulates JWA ubiquitination and promotes gastric cancer metastasis. *Biochim Biophys Acta Mol Basis Dis* 1864: 1552-1561.

3. Xie, M., et al. (2020). Exosomal circSHKBP1 promotes gastric cancer progression via regulating the miR-582-3p/HUR/VEGF axis and suppressing HSP90 degradation. *MOL CANCER* 19: 112.

Acknowledgements

We appreciate Prof. Jianwei Zhou for providing technical assistance

Conflict of Interest

The authors declare that they have no conflict of interest. All the animal experiments performed in this study were approved by the Institutional Animal Care and Use Committee of Nanjing Medical University.All animal experiments were approved by the the Institutional Animal Care and Use Committee of Nanjing Medical University. Human tissue study was approved by the Medical Ethics Committee of First Affiliated Hospital of Nanjing Medical University. Written informed consent was obtained from all participants.

Figure legends

669 **Figure. 1. miR-769-5p is enriched in BGC823/DDP cell-derived exosomes**

670 A. Double-membrane exosomes purified from the supernatants of BGC823 and
671 BGC8231/DDP cells were observed by Transmission Electron Microscopy (TEM). B.
672 NanoSight particle tracking analysis (NTA) of the diameter and concentration of
673 vesicles(particles/mL). C, D. Exosomal markers TSG101, CD9, CD81 and CD63
674 were detected by Western blot and flow cytometry (FCM) to prove that the extract in
675 exosomal protein purified from cell supernatants has the typical characteristics
676 of exosomes. E, F. Cluster heat map and Volcano plot of differential miRNAs in
677 exosomes purified from the supernatants of BGC823 and BGC823/DDP cells. G.
678 qRT-PCR verified the relative expression of miR-769-5p in exosomes purified from
679 the supernatants of BGC823, BGC823/DDP, SGC7901 and SGC7901/DDP cells. H.
680 Different expression of miR-769-5p between 41 pairs of tumor and adjacent tumor, 41
681 tumors and 346 adjacent tumors according to TCGA database. I, J. The positive rate
682 (referring to the percentage of positive cells) of miR-769-5p in 75 pairs of gastric
683 cancer tissues and adjacent tissues by RNA in situ hybridization (ISH). K. qRT-PCR
684 detected the relative expression of miR-769-5p in serum exosomes of 60 cases
685 (including 41 cisplatin-sensitive cases and 19 cisplatin-resistant cases) of GC patients.
686 After chemotherapy, the level of serum miR-769-5p was significantly increased in
687 non-response patients (n1=19) compared with response patients (n2=41). Quantitative
688 data from three independent experiments are shown as the mean ± SD (error bars).
689 *P < 0.05, **P < 0.01, ***P < 0.001 (Student's t-test)

690 **Fig're.2. Exosome-mediated transfer of miR-769-5p is required for GC**

cisplatin-resistance and targets CASP9 directly

A, B. The rates of BGC823 cells'apoptosis were reduced after being co-cultured with BD Exo (200ug/ml) for 24h and treated with cisplatin (0.4 ug/ml) for 24h detected by Hoechst nuclei staining and flow cytometry assay (FCM). C. The survival of BGC823 or SGC7901 cells co-cultured with BD Exo or SD Exo (200ug/ml) for 24h and treated with cisplatin for 24h was detected by CCK-8. D. Red fluorescence was observed in the BGC823 or SGC7901 cells after co-cultured with BGC823/DDP or SGC7901/DDP cells for 24h which were transfected with the Cy3-miR-769-5p mimic (red fluorescence). E. Confocal microscopy showed internalization of exosomes in BGC823 or SGC7901 recipient cells after co-cultured with PKH26-labeled (red fluorescence) BD Exo or SD Exo for 24h. DAPI was used to stain the nuclei of BGC823 or SGC7901 recipient cells with blue fluorescence. F. Predicted binding sites of the CASP9 3′ UTR by miR-769-5p. I. Luciferase reporter was carried out in HEK293T cotransducted with miR‐769-5p‐mimics or miRNA control with firefly luciferase reporter plasmid containing either wild-type (WT) or mutant (MUT) CASP9 3′ UTR (pGL3‐CASP9‐WT or pGL3‐CASP9‐MUT). G, H. PCR and Western blot confirmed that miR-769-5p negatively regulated the expression of CASP9. J. qRT-PCR showed the expression of miR-769-5p in in BGC anti-NC+ PBS, BGC anti-NC + BD Exo and BGC anti-769 + BD Exo. K, L. The mRNA and protein levels of CASP9 in BGC anti-NC+ PBS, BGC anti-NC + BD Exo and BGC anti-769 + BD Exo. M, N. qRT-PCR and Western blot showed the expression of miR-769-5p in BGC+BD Exo DMSO and BGC+BD Exo GW4869. O, P. The upregulation of

CASP9 mRNA and protein was detected by qRT-PCR and Western blot in BGC+BD Exo GW4869 and BGC+BD anti-769 Exo. Quantitative data from three independent experiments are shown as the mean ± SD (error bars). *P < 0.05, **P < 0.01, ***P < 0.001 (Student's t-test)

Figure.3. Exosome-mediated transfer of miR-769-5p confers cisplatin resistance through downregulating CASP9

A. Flow cytometry assay detected cell apoptosis rate of BGC anti-NC + PBS, BGC anti-NC + BD Exo, BGC anti-769 + BD Exo and BGC CASP9 + BD Exo. B. Flow cytometry assay detected cell apoptosis rate of BGC+BD Exo DMSO and BGC + BD Exo GW4869. C. Flow cytometry assay detected cell apoptosis rate of BGC + BD anti-NC Exo, BGC + BD anti-769 Exo and BGC + BD anti-769 + siCASP9 Exo. D. The level of γ-H2AX nuclear foci in BGC anti-NC + PBS, BGC anti-NC + BD Exo, BGC anti-769 + BD Exo and BGC CASP9 + BD Exo. E. The level of γ-H2AX nuclear foci in BGC+BD Exo DMSO and BGC+BD Exo GW4869. F. The level of γ-H2AX nuclear foci in BGC+BD anti-NC Exo, BGC + BD anti-769 Exo and BGC + BD anti-769 + siCASP9 Exo. G. TUNEL analysis detected cell apoptosis rate of BGC anti-NC+PBS, BGC anti-NC + BD Exo, BGC anti-769 + BD Exo and BGC CASP9 + BD Exo. Quantitative data from three independent experiments are shown as the mean ± SD (error bars). *P < 0.05, **P < 0.01, ***P < 0.001 (Student's t-test)

Figure.4. Exosomal miR-769-5p promotes recipient cells proliferation and migration by downregulating CASP9

735 A. TUNEL analysis detected cell apoptosis rate of BGC + BD Exo DMSO and BGC
736 + BD Exo GW4869. B. TUNEL analysis detected cell apoptosis rate of BGC + BD
737 anti-NC Exo, BGC + BD anti-769 Exo and BGC + BD anti-769 + siCASP9 Exo. C.
738 The average colony numbers of three independent experiments were calculated in
739 BGC anti-NC + PBS, BGC anti-NC + BD Exo, BGC anti-769 + BD Exo and BGC
740 CASP9 + BD Exo. D. The average colony numbers of three independent experiments
741 were calculated in BGC + BD Exo DMSO and BGC + BD Exo GW4869. E. The
742 average colony numbers of three independent experiments were calculated in BGC +
743 BD anti-NC Exo, BGC + BD anti-769 Exo and BGC + BD anti-769 + siCASP9 Exo.
744 F. Migration ability of BGC anti-NC + PBS, BGC anti-NC + BD Exo, BGC anti-769
745 + BD Exo and BGC CASP9 + BD Exo were assessed by Transwell assay. G.
746 Migration ability of BGC + BD Exo DMSO and BGC+BD Exo GW4869 were
747 assessed by Transwell assay. H. Migration ability of BGC+BD anti-NC Exo, BGC +
748 BD anti-769 Exo and BGC + BD anti-769 + siCASP9 Exo were assessed by
749 Transwell assay. Quantitative data from three independent experiments are shown as
750 the mean ± SD (error bars). *P < 0.05, **P < 0.01, ***P < 0.001 (Student's t-test)

751 **Figure.5. Exosomal miR-769-5p confers cisplatin resistance through**
752 **downregulating CASP9 along with subsequent evasion of apoptosis and**
753 **confirmed in vivo**

754 Western blot anaysis of caspase9, caspase3 and cleaved caspase3 in BGC + BD
755 anti-NC Exo, BGC + BD anti-769 Exo and BGC + BD anti-769 + siCASP9 Exo. B.
756 Western blot anaysis of caspase9, caspase3 and cleaved caspase3 in BGC + BD Exo

DMSO and BGC + BD Exo GW4869. C. Western blot anaysis of caspase9, caspase3 and cleaved caspase3 in BGC + BD anti-NC Exo, BGC + BD anti-769 Exo and BGC + BD anti-769 + siCASP9 Exo. D. Subcutaneous xenograft assay of BGC823 cells with or without BD Exo (200ug/100μL cells per mouse) once every two days in nude mice with PBS or cisplatin (DDP, 4mg/kg) treatment. E. Tumor volume of xenograft models were measured every two days and shown. *Tumor volume* (mm^3) = 0.5 ×$width^2$ × *length*. F. Tumor weight of xenograft models were measured every two days and shown. G. CASP9, cleaved caspase3 and p53 expression levels were shown in representative xenograft tumors by Immunohistochemistry (IHC) (400x magnification, scale bars = 50 μ m). Results are presented as mean SD. *P < 0.05, **P < 0.01, ***P < 0.001

Figure.6. miR-769-5p promotes ubiquitin-mediated p53 protein degradation in GC cells

A. KEGG enrichment analysis showed that the target genes of differentially expressed miRNAs are enriched in the p53 pathway. B. qPCR detected the expression level of p53 mRNA in BGC NC, BGC mimic-769 and BGC inhibitor-769. C. Western blot analysis of expression level of p53 protein in in BGC NC, BGC mimic-769 and BGC inhibitor-769. D. UbiBrowser website predicted E3 ubiquitination ligase with p53 as a substrate. E. Western blot analysis of p53 protein level of 100ug/ml treated with cycloheximide (CHX) changes with treatment time (0h, 1h, 4h). F. Analysis of p53 protein level by Western blot in BGC nc and BGC inhibitor-769 after treatment of MG-132 (10um) for 6h. G. Western blot analysis of

779 p53 protein expression level after transfection of E3 ubiquitinated ligase specific
780 small interfering RNA (siRNA): siFBXO11, siMIB2, siMIB1, siITCH and
781 siNEDD4L. H. Co-IP detected the interaction between NEDD4L and p53 in gastric
782 cancer cells. I. Co-IP and western blot detected p53 ubiquitination modification
783 mediated by NEDD4L. J, K. The expression of NEDD4L and p53 protein levels when
784 miR-769-5p is knocked down or overexpressed. L, M. PCR and Western blot verified
785 the negatively regulatory effects of miR-769-5p on RNF20. N. Predicted binding sites
786 of the RNF20 3′ UTR by miR-769-5p. O. Luciferase reporter was carried out in
787 HEK293T cotransducted with miR-769-5p-mimics or miRNA control with
788 pGL3-RNF20-WT or pGL3-RNF20-MUT. Quantitative data from three independent
789 experiments are shown as the mean ± SD (error bars). *P < 0.05, **P < 0.01, ***P
790 < 0.001 (Student's t-test)

791 **Figure.7. E3 ubiquitination ligase RNF20 participates in miR-769-5p mediated**
792 **p53 protein ubiquitination in GC cells**

793 A. TUNEL analysis detected cell apoptosis rate of BGC NC, BGC HA-RNF20 and
794 BGC si-RNF20. B. The level of γ -H2AX nuclear foci in BGC NC, BGC
795 HA-RNF20 and BGC si-RNF20. C. The western blot analysis of Bax, Bcl-2 and
796 cleaved caspase 3 proved the positive mediation of RNF20 on apoptosis. D, E, F. The
797 recovery proved that miR-769-5p inhibits the process of apoptosis by down-regulating
798 RNF20 by analysis of TUNEL and western blot. G, H. Flow cytometry assay proved
799 that miR-769-5p inhibits the process of apoptosis by down-regulating RNF20. I. The
800 protein levels of NEDD4L and p53 when RNF20 overexpression and knockdown. J.

Co-immunoprecipitation proves that NEDD4L interacts with RNF20. K, L. Co-immunoprecipitation proves that the ubiquitination modification of NEDD4L is mediated by RNF20 Quantitative data from three independent experiments are shown as the mean ± SD (error bars). *P < 0.05, **P < 0.01, ***P < 0.001 (Student's t-test)

Figure.8. Exosomal miR-769-5p induces cisplatin resistance and promotes the tumorigenesis of GC in vivo

A. Subcutaneous xenograft assay of BGC823/DDP cells (5×10^6 cells/100μL) with or without miR-769-5p knockdwon in nude mice with PBS or cisplatin (DDP, 4mg/kg) treatment. B. Tumor volume of xenograft models were measured every two days and shown. C. Tumor weight of xenograft models were measured every two days and shown. D. Levels of exosomal miR-769-5p in the serum were detected by qPCR. E. CASP9, cleaved caspase3 and p53 expression levels were shown in representative xenograft tumors by Immunohistochemistry (IHC) (400x magnification, scale bars = 50 μ m). F. Subcutaneous xenograft assay of BGC823 cells (5×10^6 cells/100μL) with or without miR-769-5p overexpressed in nude mice with PBS or cisplatin (DDP, 4mg/kg) treatment. G. Tumor volume of xenograft models were measured every two days and shown. H. Tumor weight of xenograft models were measured every two days and shown. I. Levels of exosomal miR-769-5p in the serum were detected by qPCR. J. CASP9, cleaved caspase3 and p53 expression levels were shown in representative xenograft tumors by Immunohistochemistry (IHC) (400x magnification, scale bars = 50 μ m). K. Summary of the mechanism by which exosomal

823 miR-769-5p induces cisplatin resistance. Results are presented as mean SD. *P < 0.05,
824 **P < 0.01, ***P < 0.001

825 **Figure.S1.** A. 5 most upregulated and downregulated miRNAs (hsa-miR-769-5p,
826 hsa-miR-30a-5p, hsa-miR-365b-3p, hsa-miR-21-3p, hsa-miR-193b-5p) were selected
827 based on the fold change and p value according to the result of differences in miRNAs
828 expressed in two cell-derived exosome populations by using sequencing analysis. B.
829 qPCR of miR-365-3p and miR-769-5p expression in exosomes released by BGC823,
830 BGC823/DDP, SGC7901, SGC7901/DDP and found that the miR-769-5p expression
831 was markedly higher in BD Exo and SD Exo. C. TCGA showed the expression of 4
832 miRNAs (hsa-miR-30a-5p, hsa-miR-365b-3p, hsa-miR-21-3p, hsa-miR-193b-5p)
833 exculding miR-769-5p in GC and adjacent normal. D. IC50 of BGC823,
834 BGC823/DDP, SGC7901, SGC7901/DDP cell lines. E. (relatead to Figure.2L) , G.
835 (relatead to Figure.2K) The mRNA and protein levels of CASP9 in SGC anti-NC+
836 PBS, SGC anti-NC + SD Exo and SGC anti-769 + SD Exo. F. (relatead to Figure.2J)
837 qRT-PCR showed the expression of miR-769-5p in in SGC anti-NC + PBS, SGC
838 anti-NC + SD Exo and SGC anti-769 + SD Exo. H. (relatead to Figure.2N), I.
839 (relatead to Figure.2M) RT-PCR and Western blot showed the expression of
840 miR-769-5p in SGC + SD Exo DMSO and SGC + SD Exo GW4869. J. (relatead to
841 Figure.2O), K. (relatead to Figure.2P) The upregulation of CASP9 mRNA and protein
842 was detected by qRT-PCR and Western blot in SGC + SD Exo GW4869 compared to
843 SGC + SD anti-769 Exo. Quantitative data from three independent experiments are
844 shown as the mean ± SD (error bars). *P < 0.05, **P < 0.01, ***P < 0.001

(Student's t-test)

Figure.S2. A. (relatead to Figure.3A) Flow cytometry assay detected cell apoptosis rate of SGC anti-NC + PBS, SGC anti-NC + SD Exo, SGC anti-769 + SD Exo and SGC CASP9 + SD Exo. B. (relatead to Figure.3B) Flow cytometry assay detected cell apoptosis rate of SGC + SD Exo DMSO and SGC + SD Exo GW4869. C. (relatead to Figure.3C) Flow cytometry assay detected cell apoptosis rate of SGC + SD anti-NC Exo, SGC + SD anti-769 Exo and SGC + SD anti-769 + siCASP9 Exo. D. (relatead to Figure.4C) The average colony numbers of three independent experiments were calculated in SGC anti-NC + PBS, SGC anti-NC + SD Exo, SGC anti-769 + SD Exo and SGCCASP9 + SD Exo. E. (relatead to Figure.4D) The average colony numbers of three independent experiments were calculated in BGC + SD Exo DMSO and BGC + SD Exo GW4869. F. (relatead to Figure.4E) The average colony numbers of three independent experiments were calculated in BGC + SD anti-NC Exo, BGC + SD anti-769 Exo and BGC + SD anti-769 + siCASP9 Exo. G. (relatead to Figure.4F) Migration and invasion ability of SGC anti-NC + PBS, SGC anti-NC+SD Exo, SGC anti-769+ SD Exo and SGCCASP9 + SD Exo were assessed by Transwell assay. H. (relatead to Figure.4G) Migration and invasion ability of BGC + SD Exo DMSO and BGC + SD Exo GW4869 were assessed by Transwell assay. I. (relatead to Figure.4H) Migration and invasion ability of BGC + SD anti-NC Exo, BGC + SD anti-769 Exo and BGC + SD anti-769 + siCASP9 Exo were assessed by Transwell assay. Quantitative data from three independent experiments are shown as the mean ± SD (error bars). *P < 0.05, **P < 0.01, ***P < 0.001 (Student's t-test)

867 **Figure.S3.** A. (relatead to Figure.3D) The level of γ-H2AX nuclear foci in SGC
868 anti-NC + PBS, SGC anti-NC + SD Exo, SGC anti-769 + SD Exo and SGC CASP9+
869 SD Exo. B. (relatead to Figure.3E) The level of γ-H2AX nuclear foci in SGC + SD
870 Exo DMSO and SGC + SD Exo GW4869. C. (relatead to Figure.3F) The level of γ
871 -H2AX nuclear foci in SGC + SD anti-NC Exo, SGC + SD anti-769 Exo and SGC +
872 SD anti-769 + siCASP9 Exo. D. (relatead to Figure.3G) TUNEL analysis detected
873 cell apoptosis rate of SGC anti-NC + PBS, SGC anti-NC + SD Exo, SGC anti-769 +
874 SD Exo and SGC CASP9 + SD Exo. E. (relatead to Figure.4A) TUNEL analysis
875 detected cell apoptosis rate of BGC + SD Exo DMSO and BGC + SD Exo GW4869.
876 F. (relatead to Figure.4B) TUNEL analysis detected cell apoptosis rate of BGC +
877 SD anti-NC Exo, BGC + SD anti-769 Exo and BGC + SD anti-769 + siCASP9 Exo.
878 Quantitative data from three independent experiments are shown as the mean ± SD
879 (error bars). *P < 0.05, **P < 0.01, ***P < 0.001 (Student's t-test)
880 **Figure.S4.** A. (relatead to Figure.5A) Western blot anaysis of caspase9, caspase3 and
881 cleaved caspase3 in SGC + SD anti-NC Exo, SGC + SD anti-769 Exo and SGC + SD
882 anti-769 + siCASP9 Exo. B. (relatead to Figure.5B) Western blot anaysis of caspase9,
883 caspase3 and cleaved caspase3 in SGC + SD Exo DMSO and SGC + SD Exo
884 GW4869. C. (relatead to Figure.5C) Western blot anysis of caspase9, caspase3 and
885 cleaved caspase3 in SGC + SD anti-NC Exo, SGC + SD anti-769 Exo and SGC +SD
886 anti-769+siCASP9 Exo. D. (relatead to Figure.6E) Western blot analysis of p53
887 protein level of 100ug/ml treated with cycloheximide (CHX) changes with treatment
888 time. E. (relatead to Figure.6F)Western blot analysis of p53 protein level after

MG-132 (10um) treatment. F. (relatead to Figure.6H) Co-IP detected the interaction between NEDD4L and p53 in SGC cells. I. Co-IP and western blot detected. G. (relatead to Figure.6I) p53 ubiquitination modification mediated by NEDD4L. H. (relatead to Figure.6J), I. (relatead to Figure.6K) The expression of NEDD4L and p53 protein levels when miR-769-5p is knocked down or overexpressed. Quantitative data from three independent experiments are shown as the mean ± SD (error bars). *P < 0.05, **P < 0.01, ***P < 0.001 (Student's t-test)

Figure.S5. A. (relatead to Figure.7A) TUNEL analysis detected cell apoptosis rate of SGC NC, SGC HA-RNF20 and SGC si-RNF20. B. (relatead to Figure.7B) The level of γ -H2AX nuclear foci in SGC NC, SGC HA-RNF20 and SGC si-RNF20. C (relatead to Figure.7D), D (relatead to Figure.7E). The recovery proved that miR-769-5p inhibits the process of apoptosis by down-regulating RNF20 by analysis of TUNEL. Quantitative data from three independent experiments are shown as the mean ± SD (error bars). *P < 0.05, **P < 0.01, ***P < 0.001 (Student's t-test)

Figure.S6. A. (relatead to Figure.7C), B (relatead to Figure.7F) The western blot analysis of Bax, Bcl-2 and cleaved caspase 3 proved the mediation of RNF20 on apoptosis. C. (relatead to Figure.7G) The protein levels of NEDD4L and p53 when RNF20 overexpression and knockdown. D. (relatead to Figure.7I) Co-IP proved that NEDD4L interacts with RNF20. E. (relatead to Figure.7J), F (relatead to Figure.7K) Co-IP proved that the ubiquitination modification of NEDD4L is mediated by RNF20. Quantitative data from three independent experiments are shown as the mean ± SD (error bars). *P < 0.05, **P < 0.01, ***P < 0.001 (Student's t-test)

911 **Tables**

912 **Table1.** Correlation of relative miR-769-5p expression with the clinicopathological

913 characteristics of 150 patients with gastric cancer.

Relationship between miR-769-5p expression and clinicopathologic factors of patients with gastric cancer				
Parameter	No. of patients	miR-769-5p(low)	miR-769-5p(high)	Pvalue (*P<0.05)
Sex				
Male	51	23	23	0.285
Female	24	14	14	
Age (year)				
<60	60	33	27	0.133
≥60	15	5	10	
Tumor size (cm)				
< 5	23	16	7	0.029
≥5	52	22	30	
Differentiation grade				
well-moderate	43	26	17	0.049
poor-undifferentiation	32	12	20	
T stage				
T1-T2	7	6	1	0.051
T3-T4	68	32	36	
Lymph node status				
Negative	23	17	6	0.007
Positive	52	21	31	
Distant metastasis				
M0	75	38	37	
M1	0	0	0	
TNM stage				
I-II	31	21	10	0.013
III-IV	44	17	27	

914 **Additional file 2: Table S1. All sequences of siRNAs are listed.**

NAME	TARGETING SEQUENCE (5′- 3′) Si-RNA1	Si-RNA2	Si-RNA3
si-CASP9	GTCGAAGCCAACCCTAGAA	GTCGAAGCCAACCCTAGAA	GCTTCGTTTCTGCGAACTA
si-TP53	GCTTCGTTTCTGCGAACTA	AGAGAATCTCCGCAAGAAA	GGAGTATTTGGATGACAGA

si-FBXO11	CCCAATTATTAGACGGAAT	AGTCCATACCAACTTCGTA	GTAGCCCTATTATTGATCA
si-MIB2	GAAGUGUGCAGAGUGUACAAAUUAU	GACUGAUGGAAUGUUUGAGACUUUA	UUCUCAUCCACAAUCCAUGGUCUUG
si-MIB1	GAACGAAGAGTGCCTTTCA	GGACAAGGATAATACCAAT	GAAGAAAGATGATGGTTAT
si-ITCH	GTATGACCTACAGGATCA	CAGCGGTATTCCAGGATTA	GATGAACCTCTTTCAGAAA
si-NEDD4L	CUUCGGUCCUGCAGUGUUA	CGACCCAGCUUGAUGGAUG	AGUCAUAAAUCUCGAGUCA
si-RNF20	GCGAATCAAGTCTAATCAG	CGCATCATCCTTAAACGTT	GGAGAGAGAACGAGAGAAA

915 **Additional file 2: Table S2. The related primers are synthesized.**

GENE	FORWARD PRIMER(5'-3')	REVERSE PRIMER(5'-3')	LOOP
hsa-miR-365b-3p	AGCCCGCCTAATGCCCCTAAAAAT	CGCAGGGTCCGAGGTATTC	GTCGTATCCAGTGCAGGGTCCGAGGTATTCGCACTGGATACGACATAAGG
hsa-miR-769-5P	ATCGGGCTGAGACCTCTGGGTTC	CGCAGGGTCCGAGGTATTC	GTCGTATCCAGTGCAGGGTCCGAGGTATTCGCACTGGATACGACAGCTCA
u6	CTCGCTTCGGCAGCACA	AACGCTTCACGAATTTGCGT	
GAPDH	CATGTGGGCCATGAGGTCCACCAC	GGGAAGCTCACTGGCATGGCCTTCC	
CASP9	CGAACTAACAGGCAAGCAGCAAAG	AGAGCACCGACATCACCAAATCC	
TP53	CAGCACATGACGGAGGTTGT	TCATCCAAATACTCCACACGC	
FBXO11	GCCGAAAAGAACAGCGTGTC	GTTTTGCACGATGACCAAAGTT	
MIB1	ATGAGTAACTCCCGGAATAACCG	GCCGTTGTCCCACACTACC	
MIB2	ACCTGCTGCTGTACGACAAC	GTGCATGTAGCACTGCGTG	
ITCH	TGATGATGGCTCCAGATCCAA	GACTCTCCTATTTTCACCAGCTC	
NEDD4L	GGGAAGCGGTGTTTTGT	CTCCTCTCCAGCCGAAT	
RNF20	GAACAGCGACTCAACCGACA	GGAATTCACCCGTTCTAGGACTT	

916 **Abbreviations**

917 gastric cancer (GC)

918 MicroRNA (miRNA)

919 ubiquitin-proteasome system (UPS)

920 NanoSight particle tracking analysis (NTA)

921 flow cytometry (FCM)

922 BGC823/DDP secreted exosomes (BD Exo)

923 BGC secreted exosomes (BC Exo)

924 tumor microenvironment (TME)

925 BGC823 cells with lentiviral vectors stably expressing miR-769-5p inhibitor (BGC
926 anti-769)

927 negative control miRNA inhibitor (BGC anti-NC)

928 BGC823 cells with lentiviral vectors stably expressing CASP9 (BGC CASP9)

929 cycloheximide (CHX)

930 small interfering RNA (siRNA)

931 Co-immunoprecipitation (CoIP)

932 **Funding**

This work was supported by grants from the Provincial Science and Technology Department Clinical Frontier Technology BE2020783(ZE20), the National Natural Science Foundation of China (No.81802381; No. 81772475; No. 81672896) and the Postgraduate Research & Practice Innovation Program of Jiangsu Province (KYCX19_1164).

References:

1. Kroemer, G., and Reed, J. C. (2000). Mitochondrial control of cell death. *NAT MED* 6: 513-519.

2. Helleday, T., Petermann, E., Lundin, C., Hodgson, B., and Sharma, R. A. (2008). DNA repair pathways as targets for cancer therapy. *NAT REV CANCER* 8: 193-204.

3. Wagner, A. D., et al. (2017). Chemotherapy for advanced gastric cancer. *Cochrane Database Syst Rev* 8: D4064.

4. Sabari, J. K., Lok, B. H., Laird, J. H., Poirier, J. T., and Rudin, C. M. (2017). Unravelling the biology of SCLC: implications for therapy. *NAT REV CLIN ONCOL* 14: 549-561.

5. Shivapurkar, N., et al. (2002). Differential inactivation of caspase-8 in lung cancers. *CANCER BIOL THER* 1: 65-69.

6. Rupaimoole, R., Calin, G. A., Lopez-Berestein, G., and Sood, A. K. (2016). miRNA Deregulation in Cancer Cells and the Tumor Microenvironment. *CANCER DISCOV* 6: 235-246.

7. Yuan, L., Xu, Z. Y., Ruan, S. M., Mo, S., Qin, J. J., and Cheng, X. D. (2020). Long non-coding RNAs towards precision medicine in gastric cancer: early diagnosis,

955 treatment, and drug resistance. *MOL CANCER* 19: 96.

956 8. Nagy, Z. B., Wichmann, B., Kalmar, A., Bartak, B. K., Tulassay, Z., and Molnar,
957 B. (2016). miRNA Isolation from FFPET Specimen: A Technical Comparison of
958 miRNA and Total RNA Isolation Methods. *PATHOL ONCOL RES* 22: 505-513.

959 9. Shi, Y. (2002). Mechanisms of caspase activation and inhibition during apoptosis.
960 *MOL CELL* 9: 459-470.

961 10. Zaslona, Z., et al. (2020). Caspase-11 promotes allergic airway inflammation.
962 *NAT COMMUN* 11: 1055.

963 11. Hanahan, D., and Weinberg, R. A. (2011). Hallmarks of cancer: the next
964 generation. *CELL* 144: 646-674.

965 12. Wu, Y., Dong, G., and Sheng, C. (2020). Targeting necroptosis in anticancer
966 therapy: mechanisms and modulators. *ACTA PHARM SIN B* 10: 1601-1618.

967 13. Eastman, A. (1990). Activation of programmed cell death by anticancer agents:
968 cisplatin as a model system. *Cancer Cells* 2: 275-280.

969 14. Gabizon, A. A., Patil, Y., and La-Beck, N. M. (2016). New insights and evolving
970 role of pegylated liposomal doxorubicin in cancer therapy. *Drug Resist Updat* 29:
971 90-106.

972 15. Hu, H. M., et al. (2018). A Quantitative Chemotherapy Genetic Interaction Map
973 Reveals Factors Associated with PARP Inhibitor Resistance. *CELL REP* 23: 918-929.

974 16. Fraser, M., Bai, T., and Tsang, B. K. (2008). Akt promotes cisplatin resistance in
975 human ovarian cancer cells through inhibition of p53 phosphorylation and nuclear
976 function. *INT J CANCER* 122: 534-546.

977 17. Liu, Z., Miers, W. R., Wei, L., and Barrett, E. J. (2000). The
978 ubiquitin-proteasome proteolytic pathway in heart vs skeletal muscle: effects of acute
979 diabetes. *Biochem Biophys Res Commun* 276: 1255-1260.
980 18. Liu, C. H., Goldberg, A. L., and Qiu, X. B. (2007). New insights into the role of
981 the ubiquitin-proteasome pathway in the regulation of apoptosis. *Chang Gung Med*
982 *J* 30: 469-479.
983 19. Vugmeyster, Y., Borodovsky, A., Maurice, M. M., Maehr, R., Furman, M. H.,
984 and Ploegh, H. L. (2002). The ubiquitin-proteasome pathway in thymocyte apoptosis:
985 caspase-dependent processing of the deubiquitinating enzyme USP7 (HAUSP). *MOL*
986 *IMMUNOL* 39: 431-441.
987 20. Daulny, A., and Tansey, W. P. (2009). Damage control: DNA repair,
988 transcription, and the ubiquitin-proteasome system. *DNA Repair (Amst)* 8: 444-448.
989 21. McBride, W. H., Iwamoto, K. S., Syljuasen, R., Pervan, M., and Pajonk, F.
990 (2003). The role of the ubiquitin/proteasome system in cellular responses to radiation.
991 *ONCOGENE* 22: 5755-5773.
992 22. Chao, C. C. (2015). Mechanisms of p53 degradation. *CLIN CHIM ACTA* 438:
993 139-147.
994 23. Kastenhuber, E. R., and Lowe, S. W. (2017). Putting p53 in Context. *CELL* 170:
995 1062-1078.
996 24. Muller, P. A., and Vousden, K. H. (2013). p53 mutations in cancer. *NAT CELL*
997 *BIOL* 15: 2-8.
998 25. Gao, S., et al. (2009). Ubiquitin ligase Nedd4L targets activated Smad2/3 to limit

TGF-beta signaling. *MOL CELL* 36: 457-468.

26. Novellasdemunt, L., et al. (2020). NEDD4 and NEDD4L regulate Wnt signalling and intestinal stem cell priming by degrading LGR5 receptor. *EMBO J* 39: e102771.

27. Wei, Y., et al. (2020). NEDD4L-mediated Merlin ubiquitination facilitates Hippo pathway activation. *EMBO REP* 21: e50642.

28. In, S., Kim, Y. I., Lee, J. E., and Kim, J. (2019). RNF20/40-mediated eEF1BdeltaL monoubiquitylation stimulates transcription of heat shock-responsive genes. *NUCLEIC ACIDS RES* 47: 2840-2855.

29. Wu, C., Cui, Y., Liu, X., Zhang, F., Lu, L. Y., and Yu, X. (2020). The RNF20/40 complex regulates p53-dependent gene transcription and mRNA splicing. *J MOL CELL BIOL* 12: 113-124.

30. Ham, I. H., et al. (2019). Targeting interleukin-6 as a strategy to overcome stroma-induced resistance to chemotherapy in gastric cancer. *MOL CANCER* 18: 68.

31. Wagner, A. D., et al. (2017). Chemotherapy for advanced gastric cancer. *Cochrane Database Syst Rev* 8: D4064.

32. Ghamloush, F., et al. (2019). The PAX3-FOXO1 oncogene alters exosome miRNA content and leads to paracrine effects mediated by exosomal miR-486. *Sci Rep* 9: 14242.

33. Huang, C., et al. (2021). Human mesenchymal stem cells promote ischemic repairment and angiogenesis of diabetic foot through exosome miRNA-21-5p. *STEM CELL RES* 52: 102235.

34. Kyuno, D., Zhao, K., Bauer, N., Ryschich, E., and Zoller, M. (2019). Therapeutic

1021 Targeting Cancer-Initiating Cell Markers by Exosome miRNA: Efficacy and
1022 Functional Consequences Exemplified for claudin7 and EpCAM. *TRANSL ONCOL*
1023 12: 191-199.
1024 35. Binenbaum, Y., et al. (2018). Transfer of miRNA in Macrophage-Derived
1025 Exosomes Induces Drug Resistance in Pancreatic Adenocarcinoma. *CANCER RES* 78:
1026 5287-5299.
1027 36. Fang, Y., et al. (2019). Exosomal miRNA-106b from cancer-associated fibroblast
1028 promotes gemcitabine resistance in pancreatic cancer. *EXP CELL RES* 383: 111543.
1029 37. Qu, L., et al. (2016). Exosome-Transmitted lncARSR Promotes Sunitinib
1030 Resistance in Renal Cancer by Acting as a Competing Endogenous RNA. *CANCER*
1031 *CELL* 29: 653-668.
1032 38. Chehab, N. H., Malikzay, A., Stavridi, E. S., and Halazonetis, T. D. (1999).
1033 Phosphorylation of Ser-20 mediates stabilization of human p53 in response to DNA
1034 damage. *Proc Natl Acad Sci U S A* 96: 13777-13782.
1035 39. Shono, T., Tofilon, P. J., Schaefer, T. S., Parikh, D., Liu, T. J., and Lang, F. F.
1036 (2002). Apoptosis induced by adenovirus-mediated p53 gene transfer in human
1037 glioma correlates with site-specific phosphorylation. *CANCER RES* 62: 1069-1076.
1038 40. Moll, U. M., and Petrenko, O. (2003). The MDM2-p53 interaction. *MOL*
1039 *CANCER RES* 1: 1001-1008.
1040 41. Zhao, K., et al. (2018). Regulation of the Mdm2-p53 pathway by the ubiquitin E3
1041 ligase MARCH7. *EMBO REP* 19: 305-319.
1042 42. Amato, R., et al. (2009). Sgk1 activates MDM2-dependent p53 degradation and

affects cell proliferation, survival, and differentiation. *J Mol Med (Berl)* 87: 1221-1239.

43. Ghosh, A., Chen, T. C., and Kapila, Y. L. (2010). Anoikis triggers Mdm2-dependent p53 degradation. *MOL CELL BIOCHEM* 343: 201-209.

44. Shema, E., et al. (2017). Corrigendum: The histone H2B-specific ubiquitin ligase RNF20/hBRE1 acts as a putative tumor suppressor through selective regulation of gene expression. *Genes Dev* 31: 1926.

45. Shema, E., et al. (2008). The histone H2B-specific ubiquitin ligase RNF20/hBRE1 acts as a putative tumor suppressor through selective regulation of gene expression. *Genes Dev* 22: 2664-2676.

Figure. 1. miR-769-5p is enriched in BGC823/DDP cell-derived exosomes

A. Double-membrane exosomes purified from the supernatants of BGC823 and BGC8231/DDP cells were observed by Transmission Electron Microscopy (TEM). B. NanoSight particle tracking analysis (NTA) of the diameter and concentration of vesicles(particles/mL). C, D. Exosomal markers TSG101, CD9, CD81 and CD63 were detected by Western blot and flow cytometry (FCM) to prove that the extract in exosomal protein purified from cell supernatants has the typical characteristics of exosomes. E, F. Cluster heat map and Volcano plot of differential miRNAs in exosomes purified from the supernatants of BGC823 and BGC823/DDP cells. G. qRT-PCR verified the relative expression of miR-769-5p in exosomes purified from the supernatants of BGC823, BGC823/DDP, SGC7901 and SGC7901/DDP cells. H. Different expression of miR-769-5p between 41 pairs of tumor and adjacent tumor, 41 tumors and 346 adjacent tumors according to TCGA database. I, J. The positive rate (referring to the percentage of positive cells) of miR-769-5p in 75 pairs of gastric cancer tissues and adjacent tissues by RNA in situ hybridization (ISH). K. qRT-PCR detected the relative expression of miR-769-5p in serum exosomes of 60 cases (including 41 cisplatin-sensitive cases and 19 cisplatin-resistant cases) of GC patients. After chemotherapy, the level of serum miR-769-5p was significantly increased in non-response patients (n1=19) compared with response patients (n2=41). Quantitative data from three independent experiments are shown as the mean ± SD (error bars). *P < 0.05, **P < 0.01, ***P < 0.001 (Student’ s t-test)

Figure.2. Exosome-mediated transfer of miR-769-5p is required for GC

cisplatin-resistance and targets CASP9 directly

A, B. The rates of BGC823 cells' apoptosis were reduced after being co-cultured with BD Exo (200ug/ml) for 24h and treated with cisplatin (0.4 ug/ml) for 24h detected by Hoechst nuclei staining and flow cytometry assay (FCM). C. The survival of BGC823 or SGC7901 cells co-cultured with BD Exo or SD Exo (200ug/ml) for 24h and treated with cisplatin for 24h was detected by CCK-8. D. Red fluorescence was observed in the BGC823 or SGC7901 cells after co-cultured with BGC823/DDP or SGC7901/DDP cells for 24h which were transfected with the Cy3-miR-769-5p mimic (red fluorescence). E. Confocal microscopy showed internalization of exosomes in BGC823 or SGC7901 recipient cells after co-cultured with PKH26-labeled (red fluorescence) BD Exo or SD Exo for 24h. DAPI was used to stain the nuclei of BGC823 or SGC7901 recipient cells with blue fluorescence. F. Predicted binding sites of the CASP9 3′ UTR by miR-769-5p. I. Luciferase reporter was carried out in HEK293T cotransducted with miR‐769-5p‐mimics or miRNA control with firefly luciferase reporter plasmid containing either wild-type (WT) or mutant (MUT) CASP9 3′ UTR (pGL3‐CASP9‐WT or pGL3‐CASP9‐MUT). G, H. PCR and Western blot confirmed that miR-769-5p negatively regulated the expression of CASP9. J. qRT-PCR showed the expression of miR-769-5p in in BGC anti-NC+ PBS, BGC anti-NC + BD Exo and BGC anti-769 + BD Exo. K, L. The mRNA and protein levels of CASP9 in BGC anti-NC+ PBS, BGC anti-NC + BD Exo and BGC anti-769 + BD Exo. M, N. qRT-PCR and Western blot showed the expression of miR-769-5p in BGC+BD Exo DMSO and BGC+BD Exo GW4869. O, P. The upregulation of CASP9

mRNA and protein was detected by qRT-PCR and Western blot in BGC+BD Exo GW4869 and BGC+BD anti-769 Exo. Quantitative data from three independent experiments are shown as the mean ± SD (error bars). *P < 0.05, **P < 0.01, ***P < 0.001 (Student' s t-test)

Figure.3. Exosome-mediated transfer of miR-769-5p confers cisplatin resistance through downregulating CASP9

A. Flow cytometry assay detected cell apoptosis rate of BGC anti-NC + PBS, BGC anti-NC + BD Exo, BGC anti-769 + BD Exo and BGC CASP9 + BD Exo. B. Flow cytometry assay detected cell apoptosis rate of BGC+BD Exo DMSO and BGC + BD Exo GW4869. C. Flow cytometry assay detected cell apoptosis rate of BGC + BD anti-NC Exo, BGC + BD anti-769 Exo and BGC + BD anti-769 + siCASP9 Exo. D. The level of γ-H2AX nuclear foci in BGC anti-NC + PBS, BGC anti-NC + BD Exo, BGC anti-769 + BD Exo and BGC CASP9 + BD Exo. E. The level of γ-H2AX nuclear foci in BGC+BD Exo DMSO and BGC+BD Exo GW4869. F. The level of γ-H2AX nuclear foci in BGC+BD anti-NC Exo, BGC + BD anti-769 Exo and BGC + BD anti-769 + siCASP9 Exo. G. TUNEL analysis detected cell apoptosis rate of BGC anti-NC+PBS, BGC anti-NC + BD Exo, BGC anti-769 + BD Exo and BGC CASP9 + BD Exo. Quantitative data from three independent experiments are shown as the mean ± SD (error bars). *P < 0.05, **P < 0.01, ***P < 0.001 (Student' s t-test)

Figure.4. Exosomal miR-769-5p promotes recipient cells proliferation and migration by downregulating CASP9

A. TUNEL analysis detected cell apoptosis rate of BGC + BD Exo DMSO and BGC

+ BD Exo GW4869. B. TUNEL analysis detected cell apoptosis rate of BGC + BD anti-NC Exo, BGC + BD anti-769 Exo and BGC + BD anti-769 + siCASP9 Exo. C. The average colony numbers of three independent experiments were calculated in BGC anti-NC + PBS, BGC anti-NC + BD Exo, BGC anti-769 + BD Exo and BGC CASP9 + BD Exo. D. The average colony numbers of three independent experiments were calculated in BGC + BD Exo DMSO and BGC + BD Exo GW4869. E. The average colony numbers of three independent experiments were calculated in BGC + BD anti-NC Exo, BGC + BD anti-769 Exo and BGC + BD anti-769 + siCASP9 Exo. F. Migration ability of BGC anti-NC + PBS, BGC anti-NC + BD Exo, BGC anti-769 + BD Exo and BGC CASP9 + BD Exo were assessed by Transwell assay. G. Migration ability of BGC + BD Exo DMSO and BGC+BD Exo GW4869 were assessed by Transwell assay. H. Migration ability of BGC+BD anti-NC Exo, BGC + BD anti-769 Exo and BGC + BD anti-769 + siCASP9 Exo were assessed by Transwell assay. Quantitative data from three independent experiments are shown as the mean ± SD (error bars). *P < 0.05, **P < 0.01, ***P < 0.001 (Student' s t-test)

Figure.5. Exosomal miR-769-5p confers cisplatin resistance through downregulating CASP9 along with subsequent evasion of apoptosis and confirmed in vivo

Western blot anaysis of caspase9, caspase3 and cleaved caspase3 in BGC + BD anti-NC Exo, BGC + BD anti-769 Exo and BGC + BD anti-769 + siCASP9 Exo. B. Western blot anaysis of caspase9, caspase3 and cleaved caspase3 in BGC + BD Exo DMSO and BGC + BD Exo GW4869. C. Western blot anaysis of caspase9, caspase3

and cleaved caspase3 in BGC + BD anti-NC Exo, BGC + BD anti-769 Exo and BGC + BD anti-769 + siCASP9 Exo. D. Subcutaneous xenograft assay of BGC823 cells with or without BD Exo (200ug/100μL cells per mouse) once every two days in nude mice with PBS or cisplatin (DDP, 4mg/kg) treatment. E. Tumor volume of xenograft models were measured every two days and shown. *Tumor volume* (mm^3) = 0.5 ×*width*^{2} × *length.* F. Tumor weight of xenograft models were measured every two days and shown. G. CASP9, cleaved caspase3 and p53 expression levels were shown in representative xenograft tumors by Immunohistochemistry (IHC) (400x magnification, scale bars = 50 μ m). Results are presented as mean SD. *P < 0.05, **P < 0.01, ***P < 0.001

Figure.6. miR-769-5p promotes ubiquitin-mediated p53 protein degradation in GC cells

A. KEGG enrichment analysis showed that the target genes of differentially expressed miRNAs are enriched in the p53 pathway. B. qPCR detected the expression level of p53 mRNA in BGC NC, BGC mimic-769 and BGC inhibitor-769. C. Western blot analysis of expression level of p53 protein in in BGC NC, BGC mimic-769 and BGC inhibitor-769. D. UbiBrowser website predicted E3 ubiquitination ligase with p53 as a substrate. E. Western blot analysis of p53 protein level of 100ug/ml treated with cycloheximide (CHX) changes with treatment time (0h, 1h, 4h). F. Analysis of p53 protein level by Western blot in BGC nc and BGC inhibitor-769 after treatment of MG-132 (10um) for 6h. G. Western blot analysis of p53 protein expression level after transfection of E3 ubiquitinated ligase specific small interfering RNA (siRNA):

siFBXO11, siMIB2, siMIB1, siITCH and siNEDD4L. H. Co-IP detected the interaction between NEDD4L and p53 in gastric cancer cells. I. Co-IP and western blot detected p53 ubiquitination modification mediated by NEDD4L. J, K. The expression of NEDD4L and p53 protein levels when miR-769-5p is knocked down or overexpressed. L, M. PCR and Western blot verified the negatively regulatory effects of miR-769-5p on RNF20. N. Predicted binding sites of the RNF20 3′ UTR by miR-769-5p. O. Luciferase reporter was carried out in HEK293T cotransducted with miR-769-5p-mimics or miRNA control with pGL3-RNF20-WT or pGL3-RNF20-MUT. Quantitative data from three independent experiments are shown as the mean ± SD (error bars). *P < 0.05, **P < 0.01, ***P < 0.001 (Student's t-test)

Figure.7. E3 ubiquitination ligase RNF20 participates in miR-769-5p mediated p53 protein ubiquitination in GC cells

A. TUNEL analysis detected cell apoptosis rate of BGC NC, BGC HA-RNF20 and BGC si-RNF20. B. The level of γ-H2AX nuclear foci in BGC NC, BGC HA-RNF20 and BGC si-RNF20. C. The western blot analysis of Bax, Bcl-2 and cleaved caspase 3 proved the positive mediation of RNF20 on apoptosis. D, E, F. The recovery proved that miR-769-5p inhibits the process of apoptosis by down-regulating RNF20 by analysis of TUNEL and western blot. G, H. Flow cytometry assay proved that miR-769-5p inhibits the process of apoptosis by down-regulating RNF20. I. The protein levels of NEDD4L and p53 when RNF20 overexpression and knockdown. J. Co-immunoprecipitation proves that NEDD4L interacts with RNF20. K, L.

Co-immunoprecipitation proves that the ubiquitination modification of NEDD4L is mediated by RNF20 Quantitative data from three independent experiments are shown as the mean ± SD (error bars). *P < 0.05, **P < 0.01, ***P < 0.001 (Student' s t-test)

Figure.8. Exosomal miR-769-5p induces cisplatin resistance and promotes the tumorigenesis of GC in vivo

A. Subcutaneous xenograft assay of BGC823/DDP cells (5 × 10^6 cells/100μL) with or without miR-769-5p knockdwon in nude mice with PBS or cisplatin (DDP, 4mg/kg) treatment. B. Tumor volume of xenograft models were measured every two days and shown. C. Tumor weight of xenograft models were measured every two days and shown. D. Levels of exosomal miR-769-5p in the serum were detected by qPCR. E. CASP9, cleaved caspase3 and p53 expression levels were shown in representative xenograft tumors by Immunohistochemistry (IHC) (400x magnification, scale bars = 50 μ m). F. Subcutaneous xenograft assay of BGC823 cells (5 × 10^6 cells/100μL) with or without miR-769-5p overexpressed in nude mice with PBS or cisplatin (DDP, 4mg/kg) treatment. G. Tumor volume of xenograft models were measured every two days and shown. H. Tumor weight of xenograft models were measured every two days and shown. I. Levels of exosomal miR-769-5p in the serum were detected by qPCR. J. CASP9, cleaved caspase3 and p53 expression levels were shown in representative xenograft tumors by Immunohistochemistry (IHC) (400x magnification, scale bars = 50 μ m). K. Summary of the mechanism by which exosomal miR-769-5p induces cisplatin resistance. Results are presented as mean SD. *P < 0.05,

**P < 0.01, ***P < 0.001

Figure.S1. A. 5 most upregulated and downregulated miRNAs (hsa-miR-769-5p, hsa-miR-30a-5p, hsa-miR-365b-3p, hsa-miR-21-3p, hsa-miR-193b-5p) were selected based on the fold change and p value according to the result of differences in miRNAs expressed in two cell-derived exosome populations by using sequencing analysis. B. qPCR of miR-365-3p and miR-769-5p expression in exosomes released by BGC823, BGC823/DDP, SGC7901, SGC7901/DDP and found that the miR-769-5p expression was markedly higher in BD Exo and SD Exo. C. TCGA showed the expression of 4 miRNAs (hsa-miR-30a-5p, hsa-miR-365b-3p, hsa-miR-21-3p, hsa-miR-193b-5p) exculding miR-769-5p in GC and adjacent normal. D. IC50 of BGC823, BGC823/DDP, SGC7901, SGC7901/DDP cell lines. E. (relatead to Figure.2L) , G. (relatead to Figure.2K) The mRNA and protein levels of CASP9 in SGC anti-NC+ PBS, SGC anti-NC + SD Exo and SGC anti-769 + SD Exo. F. (relatead to Figure.2J) qRT-PCR showed the expression of miR-769-5p in in SGC anti-NC + PBS, SGC anti-NC + SD Exo and SGC anti-769 + SD Exo. H. (relatead to Figure.2N), I. (relatead to Figure.2M) RT-PCR and Western blot showed the expression of miR-769-5p in SGC + SD Exo DMSO and SGC + SD Exo GW4869. J. (relatead to Figure.2O), K. (relatead to Figure.2P) The upregulation of CASP9 mRNA and protein was detected by qRT-PCR and Western blot in SGC + SD Exo GW4869 compared to SGC + SD anti-769 Exo. Quantitative data from three independent experiments are shown as the mean ± SD (error bars). *P < 0.05, **P < 0.01, ***P < 0.001 (Student’ s t-test)

Figure.S2. A. (relatead to Figure.3A) Flow cytometry assay detected cell apoptosis rate of SGC anti-NC + PBS, SGC anti-NC + SD Exo, SGC anti-769 + SD Exo and SGC CASP9 + SD Exo. B. (relatead to Figure.3B) Flow cytometry assay detected cell apoptosis rate of SGC + SD Exo DMSO and SGC + SD Exo GW4869. C. (relatead to Figure.3C) Flow cytometry assay detected cell apoptosis rate of SGC + SD anti-NC Exo, SGC + SD anti-769 Exo and SGC + SD anti-769 + siCASP9 Exo. D. (relatead to Figure.4C) The average colony numbers of three independent experiments were calculated in SGC anti-NC + PBS, SGC anti-NC + SD Exo, SGC anti-769 + SD Exo and SGCCASP9 + SD Exo. E. (relatead to Figure.4D) The average colony numbers of three independent experiments were calculated in BGC + SD Exo DMSO and BGC + SD Exo GW4869. F. (relatead to Figure.4E) The average colony numbers of three independent experiments were calculated in BGC + SD anti-NC Exo, BGC + SD anti-769 Exo and BGC + SD anti-769 + siCASP9 Exo. G. (relatead to Figure.4F) Migration and invasion ability of SGC anti-NC + PBS, SGC anti-NC+SD Exo, SGC anti-769+ SD Exo and SGCCASP9 + SD Exo were assessed by Transwell assay. H. (relatead to Figure.4G) Migration and invasion ability of BGC + SD Exo DMSO and BGC + SD Exo GW4869 were assessed by Transwell assay. I. (relatead to Figure.4H) Migration and invasion ability of BGC + SD anti-NC Exo, BGC + SD anti-769 Exo and BGC + SD anti-769 + siCASP9 Exo were assessed by Transwell assay. Quantitative data from three independent experiments are shown as the mean ± SD (error bars). *P < 0.05, **P < 0.01, ***P < 0.001 (Student’ s t-test)

Figure.S3. A. (relatead to Figure.3D) The level of γ -H2AX nuclear foci in SGC

anti-NC + PBS, SGC anti-NC + SD Exo, SGC anti-769 + SD Exo and SGC CASP9+ SD Exo. B. (relatead to Figure.3E) The level of γ-H2AX nuclear foci in SGC + SD Exo DMSO and SGC + SD Exo GW4869. C. (relatead to Figure.3F) The level of γ-H2AX nuclear foci in SGC + SD anti-NC Exo, SGC + SD anti-769 Exo and SGC + SD anti-769 + siCASP9 Exo. D. (relatead to Figure.3G) TUNEL analysis detected cell apoptosis rate of SGC anti-NC + PBS, SGC anti-NC + SD Exo, SGC anti-769 + SD Exo and SGC CASP9 + SD Exo. E. (relatead to Figure.4A) TUNEL analysis detected cell apoptosis rate of BGC + SD Exo DMSO and BGC + SD Exo GW4869. F. (relatead to Figure.4B) TUNEL analysis detected cell apoptosis rate of BGC + SD anti-NC Exo, BGC + SD anti-769 Exo and BGC + SD anti-769 + siCASP9 Exo. Quantitative data from three independent experiments are shown as the mean ± SD (error bars). *P < 0.05, **P < 0.01, ***P < 0.001 (Student's t-test)

Figure.S4. A. (relatead to Figure.5A) Western blot anaysis of caspase9, caspase3 and cleaved caspase3 in SGC + SD anti-NC Exo, SGC + SD anti-769 Exo and SGC + SD anti-769 + siCASP9 Exo. B. (relatead to Figure.5B) Western blot anaysis of caspase9, caspase3 and cleaved caspase3 in SGC + SD Exo DMSO and SGC + SD Exo GW4869. C. (relatead to Figure.5C) Western blot anysis of caspase9, caspase3 and cleaved caspase3 in SGC + SD anti-NC Exo, SGC + SD anti-769 Exo and SGC +SD anti-769+siCASP9 Exo. D. (relatead to Figure.6E) Western blot analysis of p53 protein level of 100ug/ml treated with cycloheximide (CHX) changes with treatment time. E. (relatead to Figure.6F)Western blot analysis of p53 protein level after MG-132 (10um) treatment. F. (relatead to Figure.6H) Co-IP detected the interaction

between NEDD4L and p53 in SGC cells. I. Co-IP and western blot detected. G. (relatead to Figure.6I) p53 ubiquitination modification mediated by NEDD4L. H. (relatead to Figure.6J), I. (relatead to Figure.6K) The expression of NEDD4L and p53 protein levels when miR-769-5p is knocked down or overexpressed. Quantitative data from three independent experiments are shown as the mean ± SD (error bars). *P < 0.05, **P < 0.01, ***P < 0.001 (Student' s t-test)

Figure.S5. A. (relatead to Figure.7A) TUNEL analysis detected cell apoptosis rate of SGC NC, SGC HA-RNF20 and SGC si-RNF20. B. (relatead to Figure.7B) The level of γ -H2AX nuclear foci in SGC NC, SGC HA-RNF20 and SGC si-RNF20. C (relatead to Figure.7D), D (relatead to Figure.7E). The recovery proved that miR-769-5p inhibits the process of apoptosis by down-regulating RNF20 by analysis of TUNEL. Quantitative data from three independent experiments are shown as the mean ± SD (error bars). *P < 0.05, **P < 0.01, ***P < 0.001 (Student' s t-test)

Figure.S6. A. (relatead to Figure.7C), B (relatead to Figure.7F) The western blot analysis of Bax, Bcl-2 and cleaved caspase 3 proved the mediation of RNF20 on apoptosis. C. (relatead to Figure.7G) The protein levels of NEDD4L and p53 when RNF20 overexpression and knockdown. D. (relatead to Figure.7I) Co-IP proved that NEDD4L interacts with RNF20. E. (relatead to Figure.7J), F (relatead to Figure.7K) Co-IP proved that the ubiquitination modification of NEDD4L is mediated by RNF20. Quantitative data from three independent experiments are shown as the mean ± SD (error bars). *P < 0.05, **P < 0.01, ***P < 0.001 (Student' s t-test)

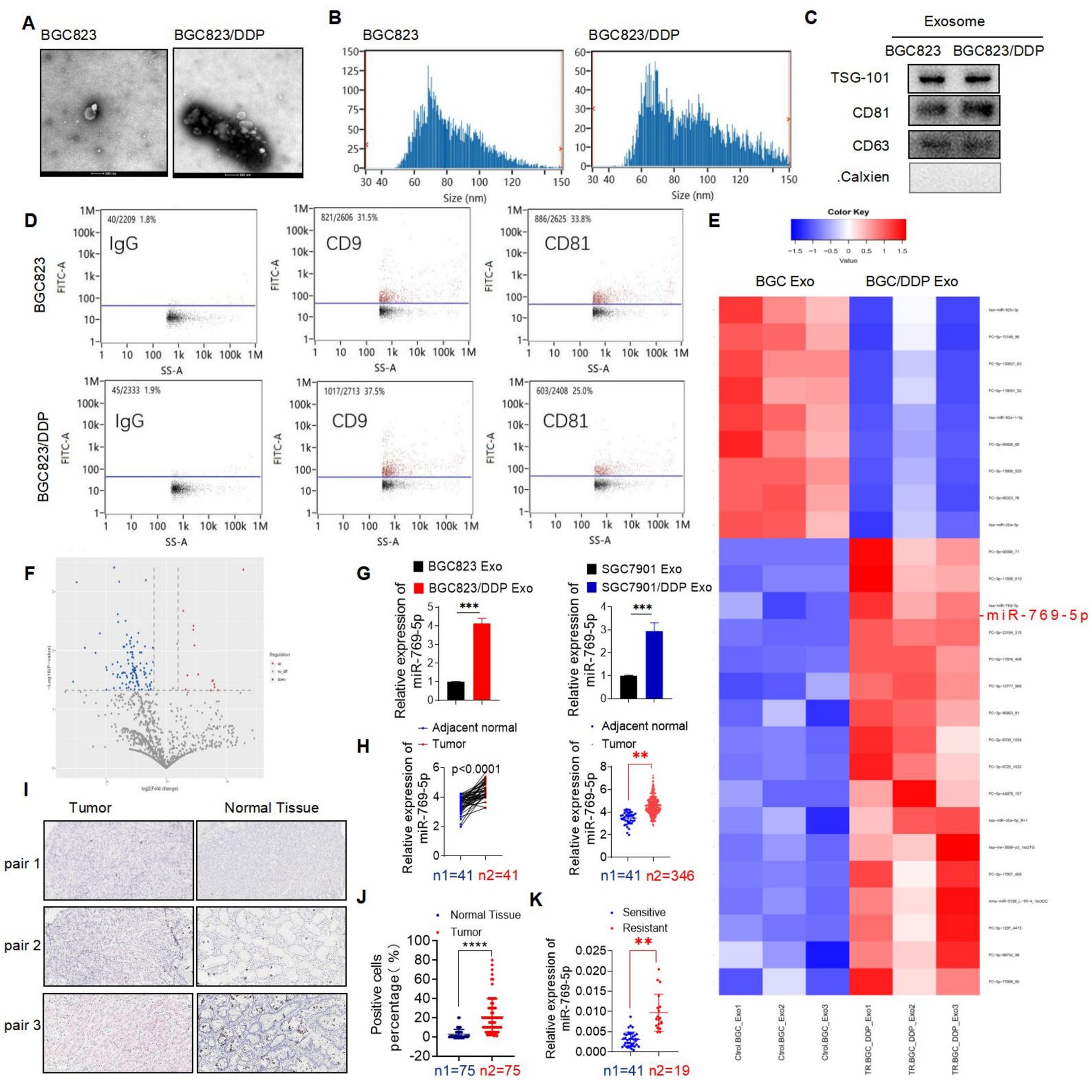
A
BGC823
BGC823/DDP
B
BGC823
BGC823/DDP
Size (nm)
C
Exosome
BGC823
BGC823/DDP
TSG-101
CD81
CD63
.Calxien
D
BGC823
BGC823/DDP
IgG
CD9
CD81
40/2209 1.8%
821/2606 31.5%
886/2625 33.8%
45/2333 1.9%
1017/2713 37.5%
603/2408 25.0%
FITC-A
SS-A
E
Color Key
Value
BGC Exo
BGC/DDP Exo
miR-769-5p
Ctrol.BGC_Exo1
Ctrol.BGC_Exo2
Ctrol.BGC_Exo3
TR.BGC_DDP_Exo1
TR.BGC_DDP_Exo2
TR.BGC_DDP_Exo3
F
log2(Fold change)
G
BGC823 Exo
BGC823/DDP Exo
SGC7901 Exo
SGC7901/DDP Exo
Relative expression of miR-769-5p
H
Adjacent normal
Tumor
p<0.0001
n1=41 n2=41
n1=41 n2=346
I
Tumor
Normal Tissue
pair 1
pair 2
pair 3
J
Normal Tissue
Tumor
Positive cells percentage (%)
n1=75 n2=75
K
Sensitive
Resistant
n1=41 n2=19

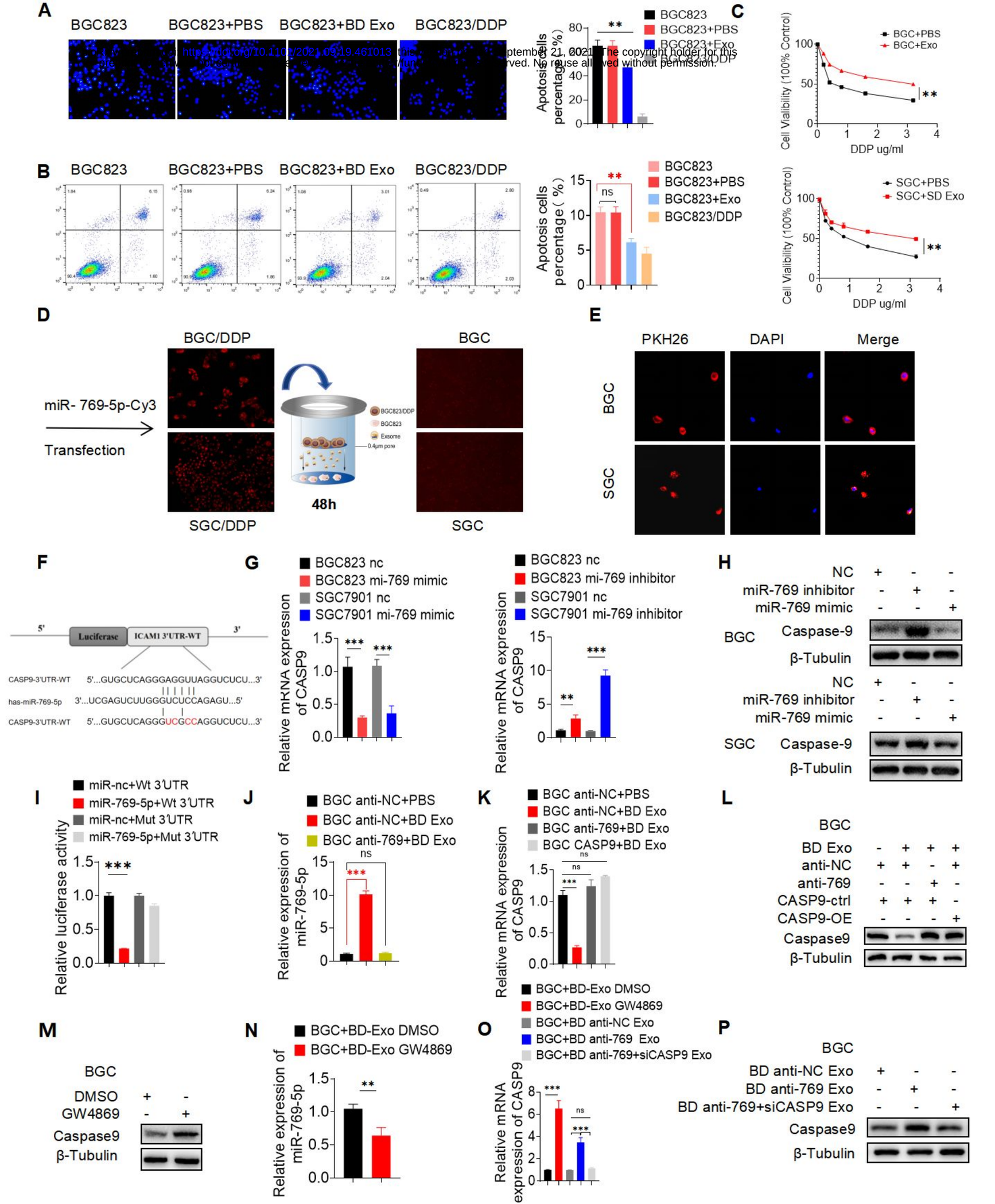

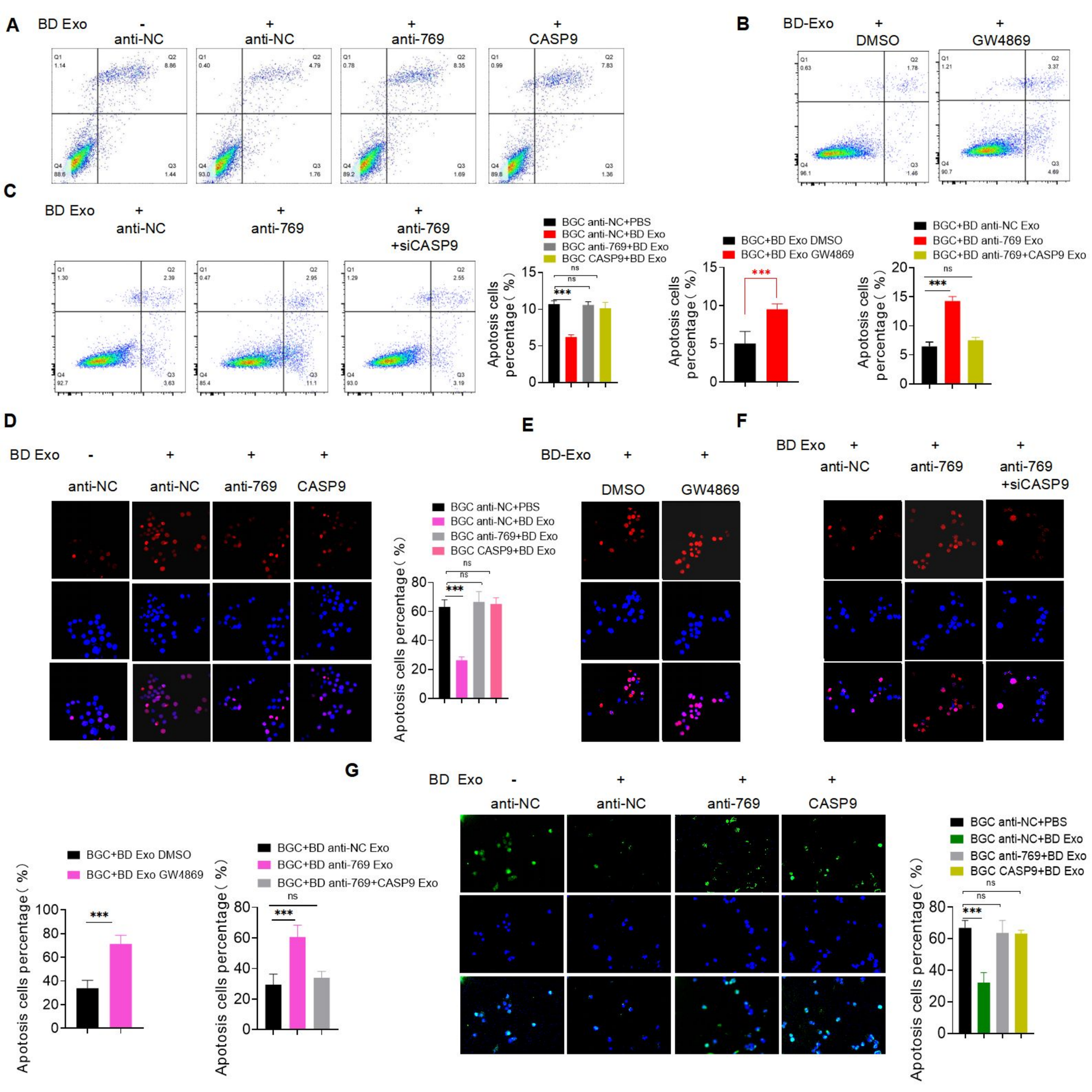
A
BD Exo
-
anti-NC
+
anti-NC
+
anti-769
+
CASP9
B
BD-Exo
+
DMSO
+
GW4869
C
BD Exo
+
anti-NC
+
anti-769
+
anti-769
+siCASP9
BGC anti-NC+PBS
BGC anti-NC+BD Exo
BGC anti-769+BD Exo
BGC CASP9+BD Exo
Apotosis cells percentage (%)
BGC+BD Exo DMSO
BGC+BD Exo GW4869
BGC+BD anti-NC Exo
BGC+BD anti-769 Exo
BGC+BD anti-769+CASP9 Exo
D
BD Exo
-
+
+
+
anti-NC
anti-NC
anti-769
CASP9
Apotosis cells percentage (%)
E
BD-Exo
+
+
DMSO
GW4869
F
BD Exo
+
+
+
anti-NC
anti-769
anti-769
+siCASP9
G
BD Exo
-
+
+
+
anti-NC
anti-NC
anti-769
CASP9
BGC anti-NC+PBS
BGC anti-NC+BD Exo
BGC anti-769+BD Exo
BGC CASP9+BD Exo
Apotosis cells percentage (%)

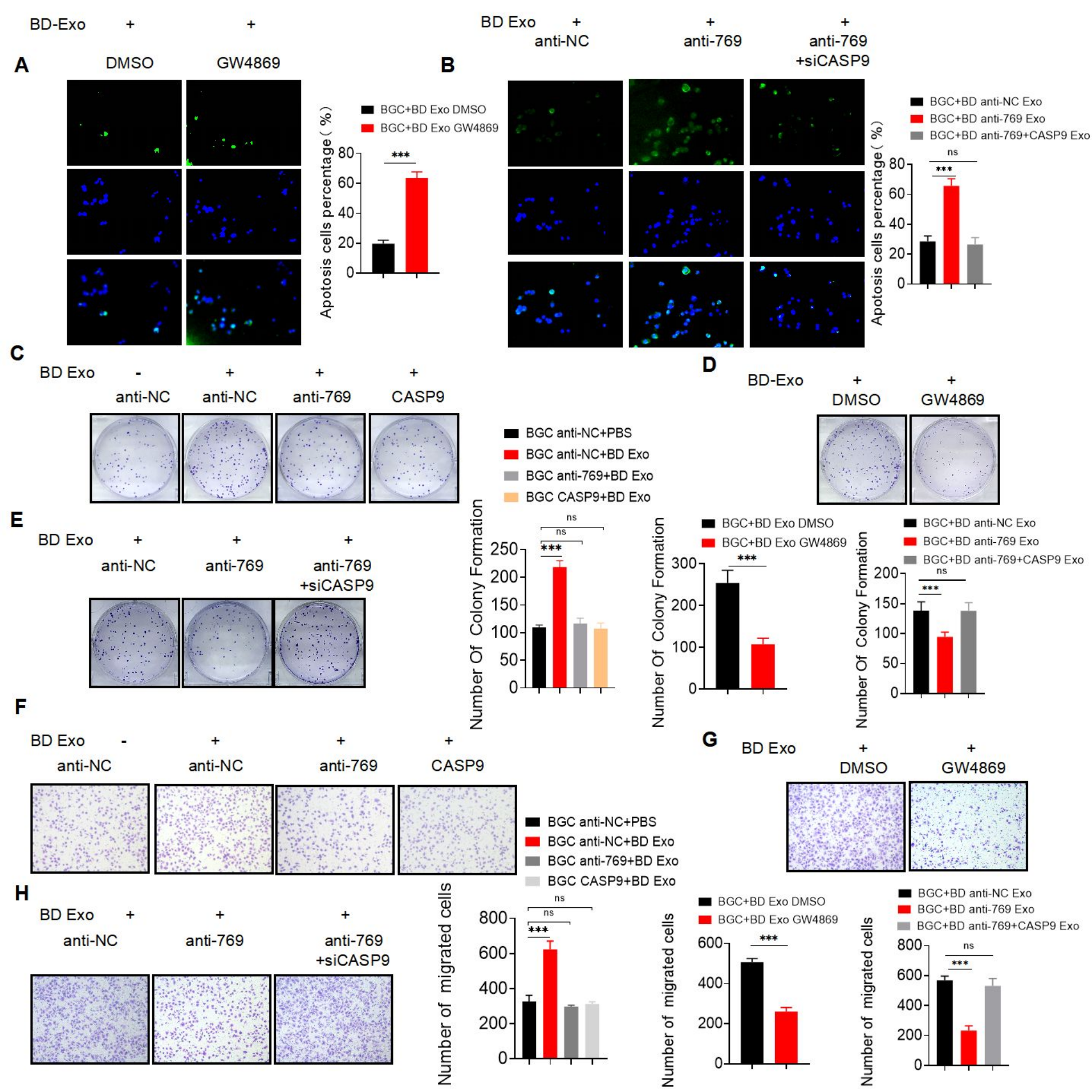
BD-Exo + +
DMSO GW4869
A
BGC+BD Exo DMSO
BGC+BD Exo GW4869
Apotosis cells percentage (%)
***
BD Exo + + +
anti-NC anti-769 anti-769 +siCASP9
B
BGC+BD anti-NC Exo
BGC+BD anti-769 Exo
BGC+BD anti-769+CASP9 Exo
ns
***
C
BD Exo - + + +
anti-NC anti-NC anti-769 CASP9
BGC anti-NC+PBS
BGC anti-NC+BD Exo
BGC anti-769+BD Exo
BGC CASP9+BD Exo
D
BD-Exo + +
DMSO GW4869
E
BD Exo + + +
anti-NC anti-769 anti-769 +siCASP9
Number Of Colony Formation
ns
***
F
BD Exo - + + +
anti-NC anti-NC anti-769 CASP9
Number of migrated cells
G
BD Exo + +
DMSO GW4869
H
BD Exo + + +
anti-NC anti-769 anti-769 +siCASP9

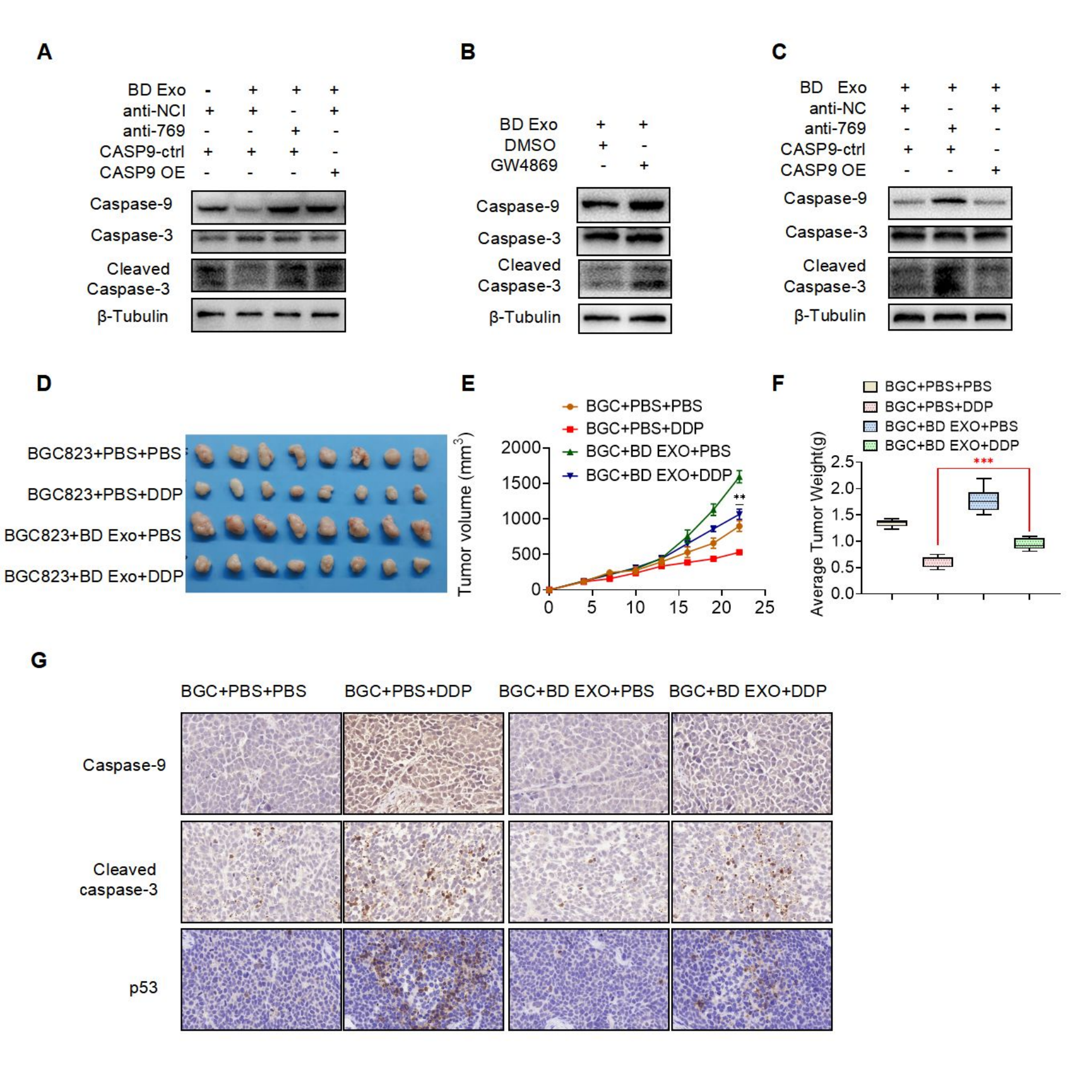
A
BD Exo - + + +
anti-NCI + + - +
anti-769 - - + -
CASP9-ctrl + + + -
CASP9 OE - - - +
Caspase-9
Caspase-3
Cleaved Caspase-3
β-Tubulin
B
BD Exo + +
DMSO + -
GW4869 - +
Caspase-9
Caspase-3
Cleaved Caspase-3
β-Tubulin
C
BD Exo + + +
anti-NC + - +
anti-769 - + -
CASP9-ctrl + + -
CASP9 OE - - +
Caspase-9
Caspase-3
Cleaved Caspase-3
β-Tubulin
D
BGC823+PBS+PBS
BGC823+PBS+DDP
BGC823+BD Exo+PBS
BGC823+BD Exo+DDP
E
BGC+PBS+PBS
BGC+PBS+DDP
BGC+BD EXO+PBS
BGC+BD EXO+DDP
Tumor volume (mm3)
2000
1500
1000
500
0
0 5 10 15 20 25
**
F
BGC+PBS+PBS
BGC+PBS+DDP
BGC+BD EXO+PBS
BGC+BD EXO+DDP
Average Tumor Weight(g)
2.5
2.0
1.5
1.0
0.5
0.0
***
G
BGC+PBS+PBS
BGC+PBS+DDP
BGC+BD EXO+PBS
BGC+BD EXO+DDP
Caspase-9
Cleaved caspase-3
p53

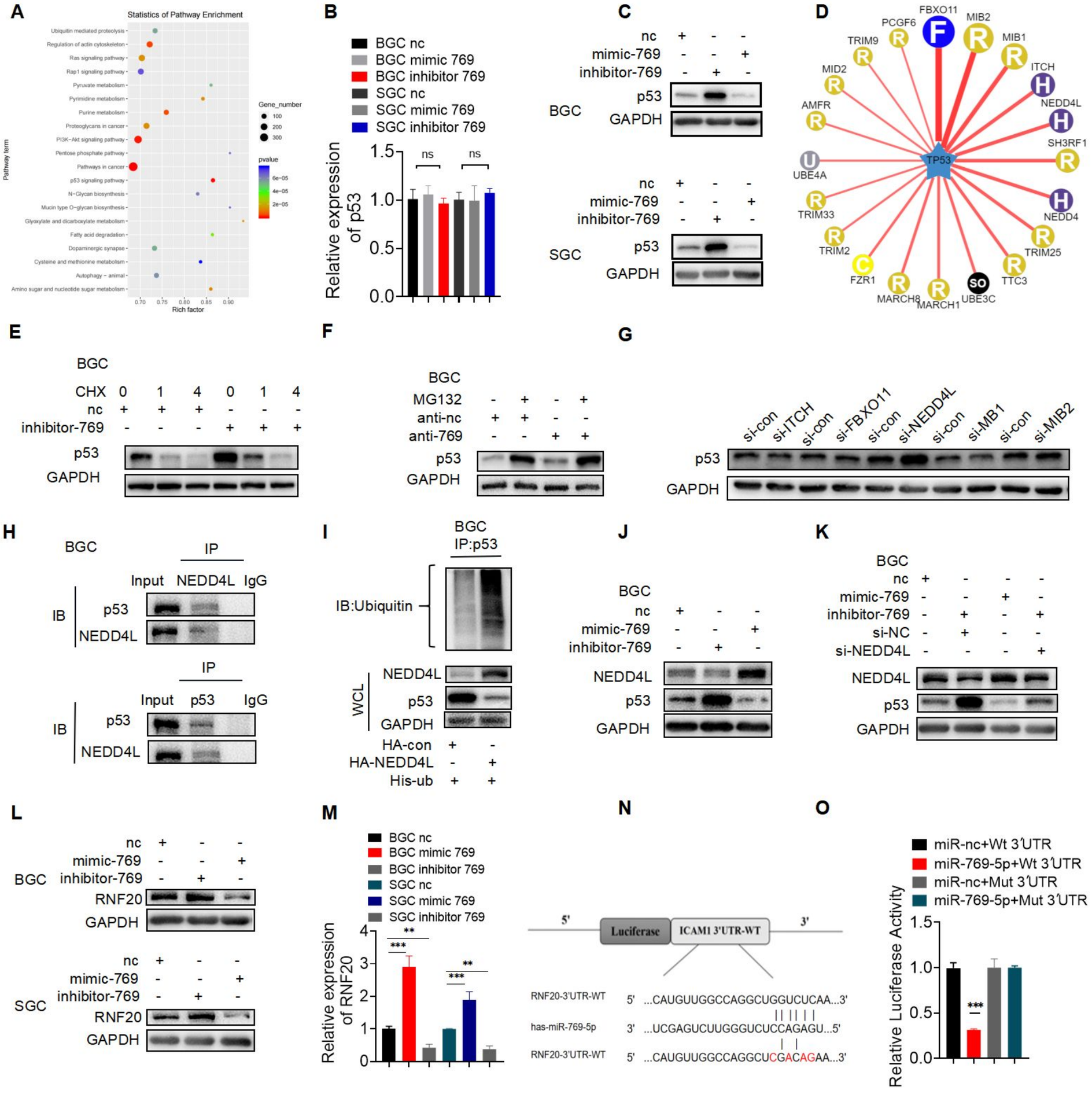
A
Statistics of Pathway Enrichment
Ubiquitin mediated proteolysis
Regulation of actin cytoskeleton
Ras signaling pathway
Rap1 signaling pathway
Pyruvate metabolism
Pyrimidine metabolism
Purine metabolism
Proteoglycans in cancer
PI3K−Akt signaling pathway
Pentose phosphate pathway
Pathways in cancer
p53 signaling pathway
N−Glycan biosynthesis
Mucin type O−glycan biosynthesis
Glyoxylate and dicarboxylate metabolism
Fatty acid degradation
Dopaminergic synapse
Cysteine and methionine metabolism
Autophagy − animal
Amino sugar and nucleotide sugar metabolism
Pathway term
Rich factor
Gene_number
pvalue
B
BGC nc
BGC mimic 769
BGC inhibitor 769
SGC nc
SGC mimic 769
SGC inhibitor 769
Relative expression of p53
ns
C
nc
mimic-769
inhibitor-769
BGC
SGC
p53
GAPDH
D
FBXO11
PCGF6
MIB2
MIB1
TRIM9
ITCH
MID2
NEDD4L
AMFR
SH3RF1
TP53
UBE4A
TRIM33
NEDD4
TRIM2
TRIM25
FZR1
TTC3
MARCH8
MARCH1
UBE3C
E
BGC
CHX 0 1 4 0 1 4
nc
inhibitor-769
p53
GAPDH
F
BGC
MG132
anti-nc
anti-769
p53
GAPDH
G
si-con
si-ITCH
si-FBXO11
si-NEDD4L
si-MB1
si-MIB2
p53
GAPDH
H
BGC
IP
Input NEDD4L IgG
IB
p53
NEDD4L
Input p53 IgG
I
BGC
IP:p53
IB:Ubiquitin
WCL
NEDD4L
p53
GAPDH
HA-con
HA-NEDD4L
His-ub
J
BGC
nc
mimic-769
inhibitor-769
NEDD4L
p53
GAPDH
K
BGC
nc
mimic-769
inhibitor-769
si-NC
si-NEDD4L
NEDD4L
p53
GAPDH
L
BGC
nc
mimic-769
inhibitor-769
RNF20
GAPDH
SGC
M
BGC nc
BGC mimic 769
BGC inhibitor 769
SGC nc
SGC mimic 769
SGC inhibitor 769
Relative expression of RNF20
N
5'
Luciferase
ICAM1 3'UTR-WT
3'
RNF20-3'UTR-WT 5' ...CAUGUUGGCCAGGCUGGUCUCAA...3'
has-miR-769-5p 3' ...UCGAGUCUUGGGUCUCCAGAGU...5'
RNF20-3'UTR-WT 5' ...CAUGUUGGCCAGGCUCGACAGAA...3'
O
miR-nc+Wt 3′UTR
miR-769-5p+Wt 3′UTR
miR-nc+Mut 3′UTR
miR-769-5p+Mut 3′UTR
Relative Luciferase Activity

https://doi.org/10.1101/2021.09.19.461013 this version posted September 21, 2021. The copyright holder for this preprint

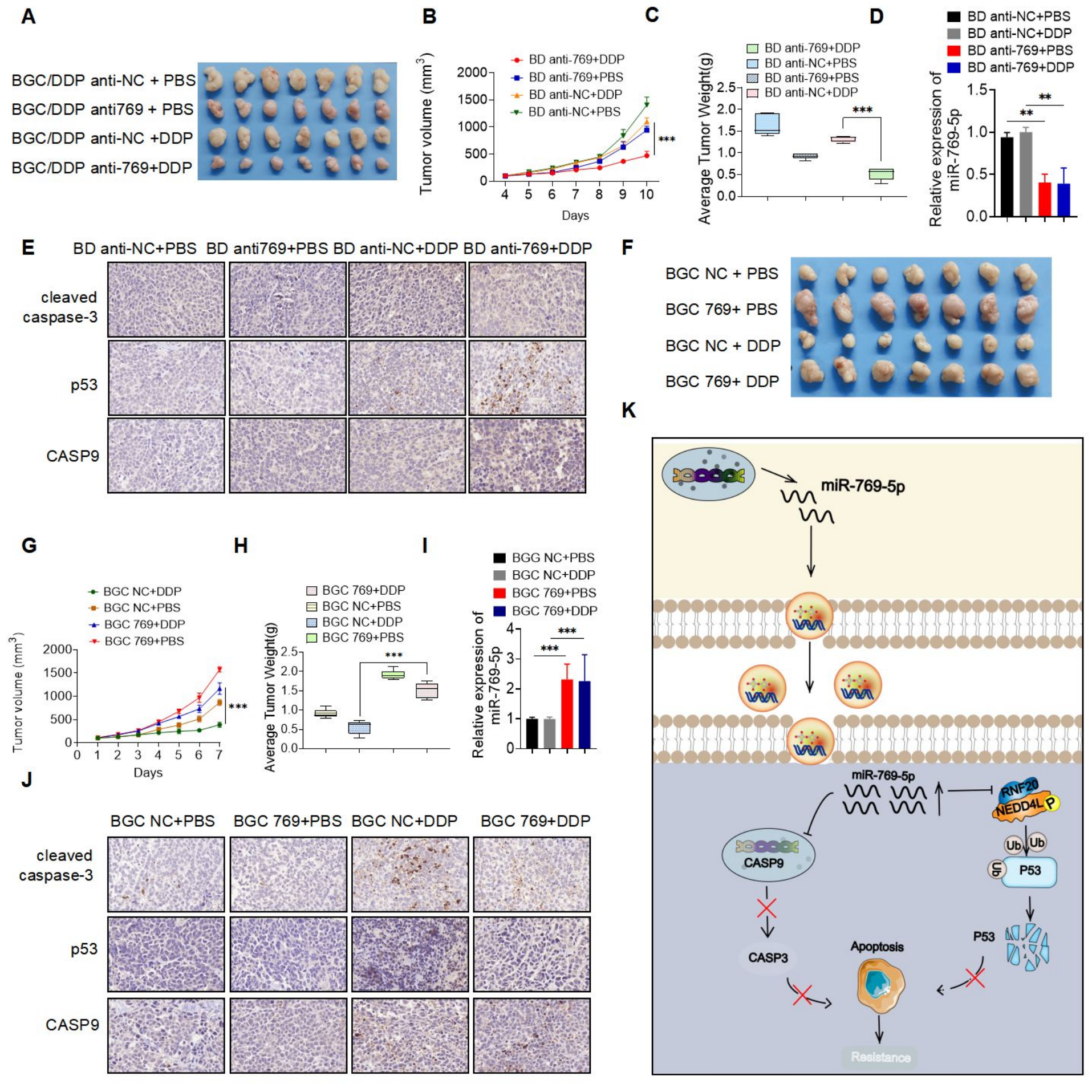
A
BGC/DDP anti-NC + PBS
BGC/DDP anti769 + PBS
BGC/DDP anti-NC +DDP
BGC/DDP anti-769+DDP
B
Tumor volume (mm3)
BD anti-769+DDP
BD anti-769+PBS
BD anti-NC+DDP
BD anti-NC+PBS
***
Days
C
Average Tumor Weight(g)
BD anti-769+DDP
BD anti-NC+PBS
BD anti-769+PBS
BD anti-NC+DDP
***
D
BD anti-NC+PBS
BD anti-NC+DDP
BD anti-769+PBS
BD anti-769+DDP
Relative expression of miR-769-5p
**
**
E
BD anti-NC+PBS
BD anti769+PBS
BD anti-NC+DDP
BD anti-769+DDP
cleaved caspase-3
p53
CASP9
F
BGC NC + PBS
BGC 769+ PBS
BGC NC + DDP
BGC 769+ DDP
G
BGC NC+DDP
BGC NC+PBS
BGC 769+DDP
BGC 769+PBS
Tumor volume (mm3)
***
Days
H
BGC 769+DDP
BGC NC+PBS
BGC NC+DDP
BGC 769+PBS
Average Tumor Weight(g)
***
I
BGG NC+PBS
BGC NC+DDP
BGC 769+PBS
BGC 769+DDP
Relative expression of miR-769-5p
***
***
J
BGC NC+PBS
BGC 769+PBS
BGC NC+DDP
BGC 769+DDP
cleaved caspase-3
p53
CASP9
K
miR-769-5p
miR-769-5p
RNF20
NEDD4L
Ub
Ub
P53
CASP9
CASP3
Apoptosis
P53
Resistance

A

miR_name	up/down	fold_change	pvalue(t_test)
hsa-miR-769-5p	up	4.77	4.45E-03
hsa-miR-30a-5p_R+1	up	1.89	7.70E-03
hsa-miR-365b-3p	down	0.05	3.87E-04
hsa-miR-21-3p_R+1	down	0.31	6.35E-04
hsa-miR-193b-1-5p	down	0.10	3.13E-03

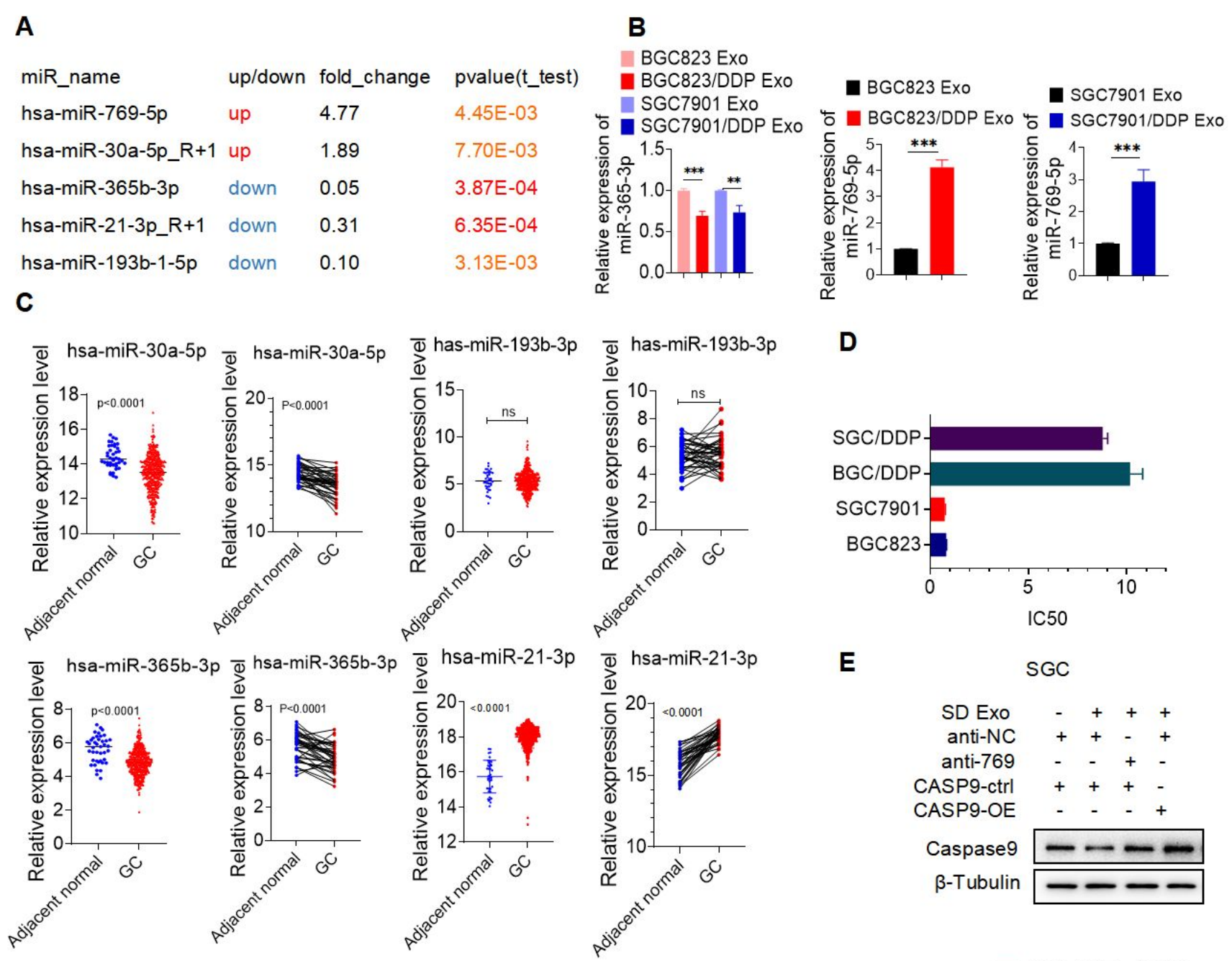

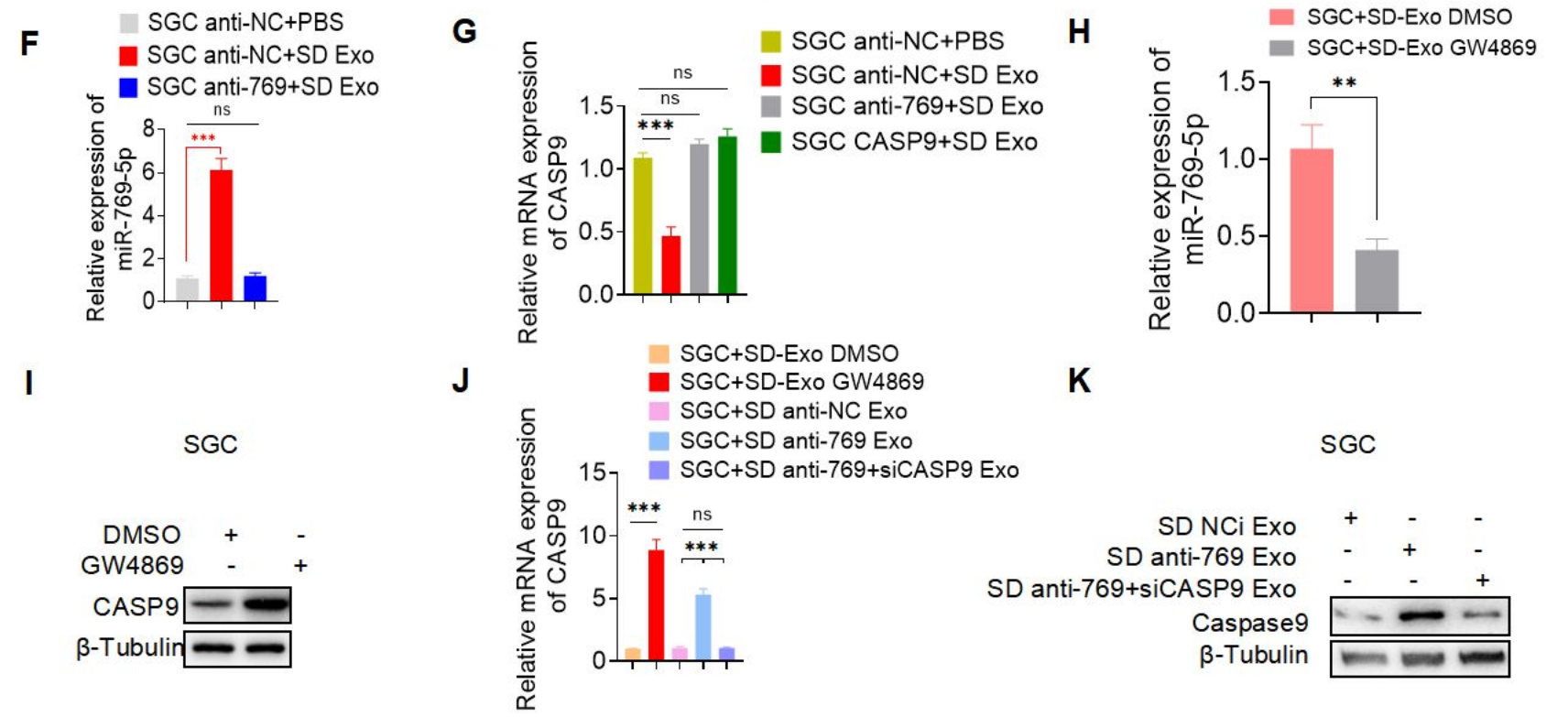

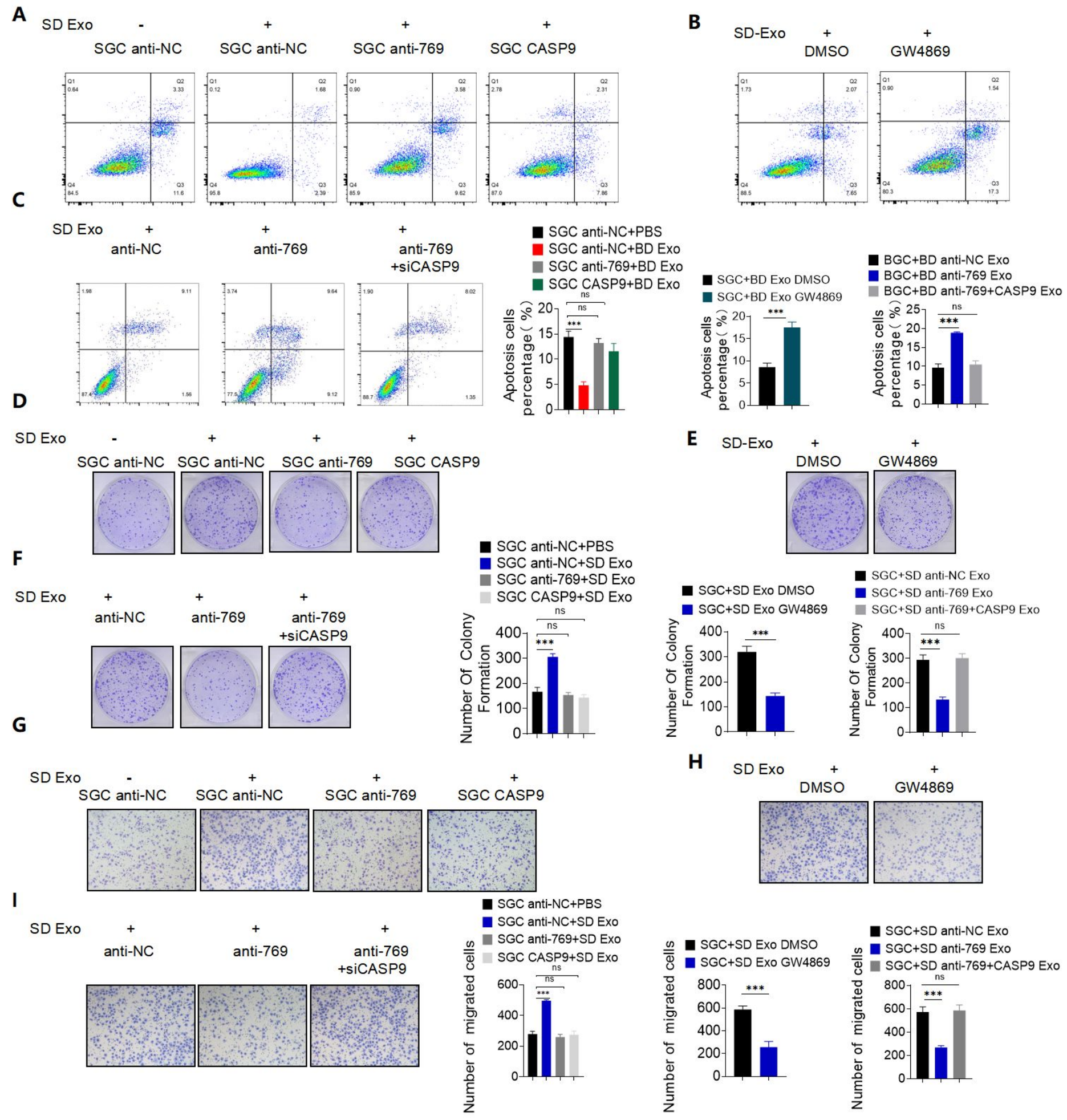
A
SD Exo - + + +
SGC anti-NC
SGC anti-NC
SGC anti-769
SGC CASP9
B
SD-Exo + +
DMSO
GW4869
C
SD Exo + + +
anti-NC
anti-769
anti-769 +siCASP9
SGC anti-NC+PBS
SGC anti-NC+BD Exo
SGC anti-769+BD Exo
SGC CASP9+BD Exo
Apotosis cells percentage(%)
SGC+BD Exo DMSO
SGC+BD Exo GW4869
BGC+BD anti-NC Exo
BGC+BD anti-769 Exo
BGC+BD anti-769+CASP9 Exo
D
SD Exo - + + +
SGC anti-NC
SGC anti-NC
SGC anti-769
SGC CASP9
E
SD-Exo + +
DMSO
GW4869
F
SD Exo + + +
anti-NC
anti-769
anti-769 +siCASP9
SGC anti-NC+PBS
SGC anti-NC+SD Exo
SGC anti-769+SD Exo
SGC CASP9+SD Exo
Number Of Colony Formation
SGC+SD Exo DMSO
SGC+SD Exo GW4869
SGC+SD anti-NC Exo
SGC+SD anti-769 Exo
SGC+SD anti-769+CASP9 Exo
G
SD Exo - + + +
SGC anti-NC
SGC anti-NC
SGC anti-769
SGC CASP9
H
SD Exo + +
DMSO
GW4869
I
SD Exo + + +
anti-NC
anti-769
anti-769 +siCASP9
SGC anti-NC+PBS
SGC anti-NC+SD Exo
SGC anti-769+SD Exo
SGC CASP9+SD Exo
Number of migrated cells
SGC+SD Exo DMSO
SGC+SD Exo GW4869
SGC+SD anti-NC Exo
SGC+SD anti-769 Exo
SGC+SD anti-769+CASP9 Exo

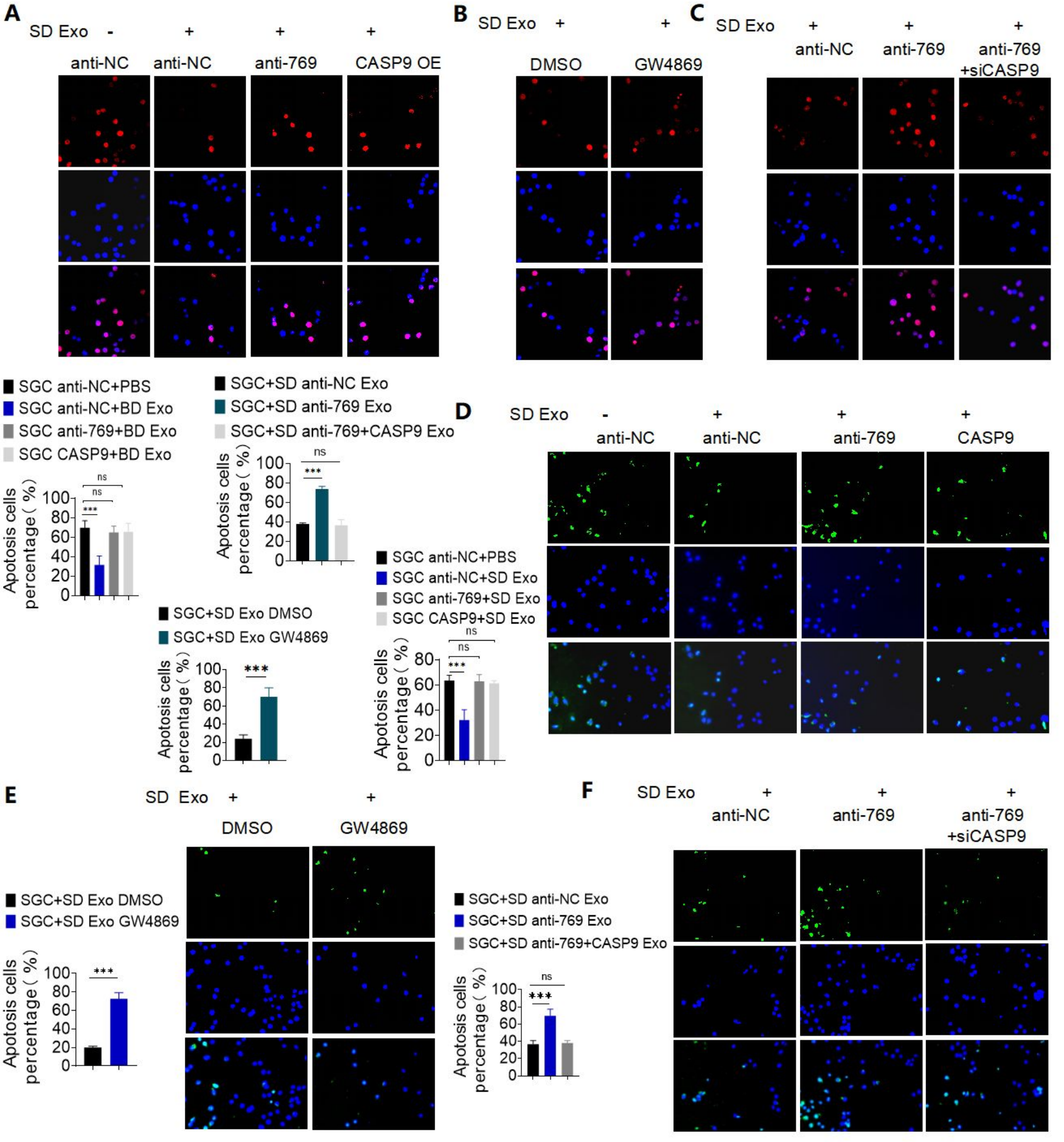
A
SD Exo - + + +
anti-NC anti-NC anti-769 CASP9 OE
B
SD Exo + +
DMSO GW4869
C
SD Exo + + +
anti-NC anti-769 anti-769 +siCASP9
SGC anti-NC+PBS
SGC anti-NC+BD Exo
SGC anti-769+BD Exo
SGC CASP9+BD Exo
Apotosis cells percentage (%)
ns
***
SGC+SD anti-NC Exo
SGC+SD anti-769 Exo
SGC+SD anti-769+CASP9 Exo
SGC+SD Exo DMSO
SGC+SD Exo GW4869
D
SD Exo - + + +
anti-NC anti-NC anti-769 CASP9
SGC anti-NC+SD Exo
SGC anti-769+SD Exo
SGC CASP9+SD Exo
E
SD Exo + +
DMSO GW4869
F
SD Exo + + +
anti-NC anti-769 anti-769 +siCASP9

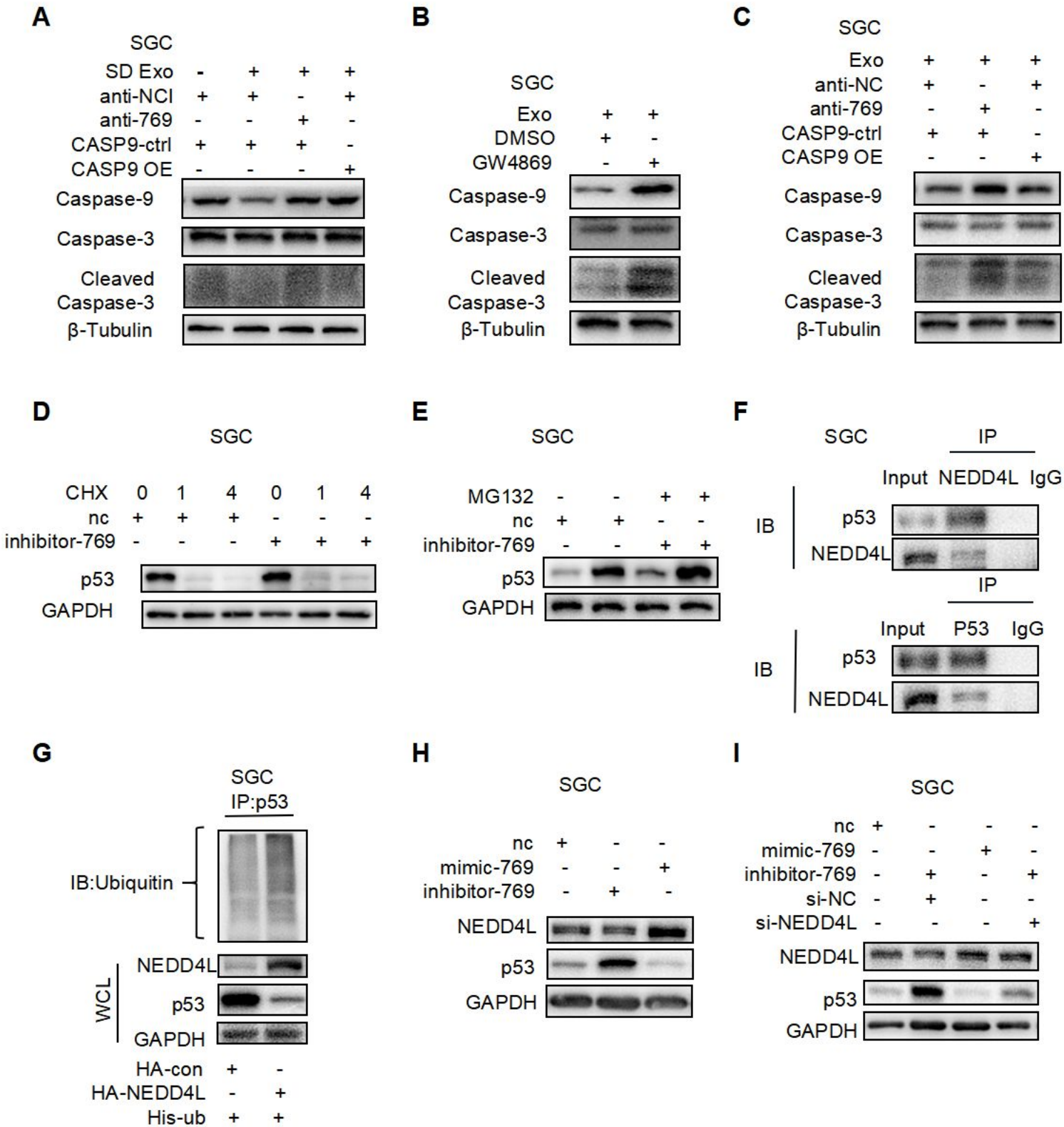
A
SGC
SD Exo - + + +
anti-NCI + + - +
anti-769 - - + -
CASP9-ctrl + + + -
CASP9 OE - - - +
Caspase-9
Caspase-3
Cleaved Caspase-3
β-Tubulin
B
SGC
Exo + +
DMSO + -
GW4869 - +
Caspase-9
Caspase-3
Cleaved Caspase-3
β-Tubulin
C
SGC
Exo + + +
anti-NC + - +
anti-769 - + -
CASP9-ctrl + + -
CASP9 OE - - +
Caspase-9
Caspase-3
Cleaved Caspase-3
β-Tubulin
D
SGC
CHX 0 1 4 0 1 4
nc + + + - - -
inhibitor-769 - - - + + +
p53
GAPDH
E
SGC
MG132 - - + +
nc + + - -
inhibitor-769 - - + +
p53
GAPDH
F
SGC
IP
Input NEDD4L IgG
IB
p53
NEDD4L
IP
Input P53 IgG
IB
p53
NEDD4L
G
SGC
IP:p53
IB:Ubiquitin
WCL
NEDD4L
p53
GAPDH
HA-con + -
HA-NEDD4L - +
His-ub + +
H
SGC
nc + - -
mimic-769 - - +
inhibitor-769 - + -
NEDD4L
p53
GAPDH
I
SGC
nc + - - -
mimic-769 - - + -
inhibitor-769 - + - +
si-NC - + - -
si-NEDD4L - - - +
NEDD4L
p53
GAPDH

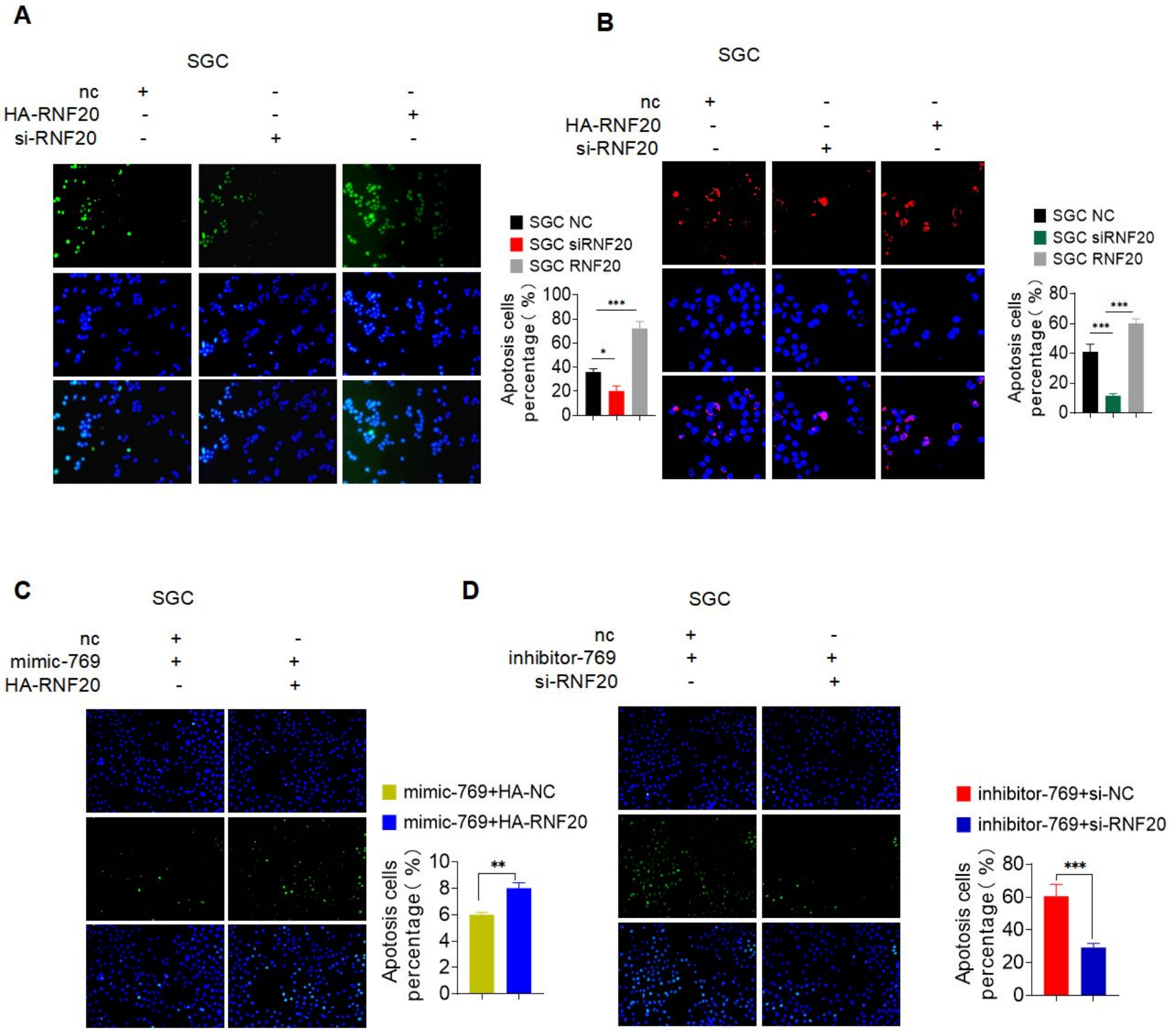
A
SGC
nc + - -
HA-RNF20 - - +
si-RNF20 - + -
B
SGC
nc + - -
HA-RNF20 - - +
si-RNF20 - + -
SGC NC
SGC siRNF20
SGC RNF20
Apotosis cells percentage (%)
100
80
60
40
20
0
*
***
SGC NC
SGC siRNF20
SGC RNF20
Apotosis cells percentage (%)
80
60
40
20
0
***
***
C
SGC
nc + -
mimic-769 + +
HA-RNF20 - +
mimic-769+HA-NC
mimic-769+HA-RNF20
Apotosis cells percentage (%)
10
8
6
4
2
0
**
D
SGC
nc + -
inhibitor-769 + +
si-RNF20 - +
inhibitor-769+si-NC
inhibitor-769+si-RNF20
Apotosis cells percentage (%)
80
60
40
20
0
***

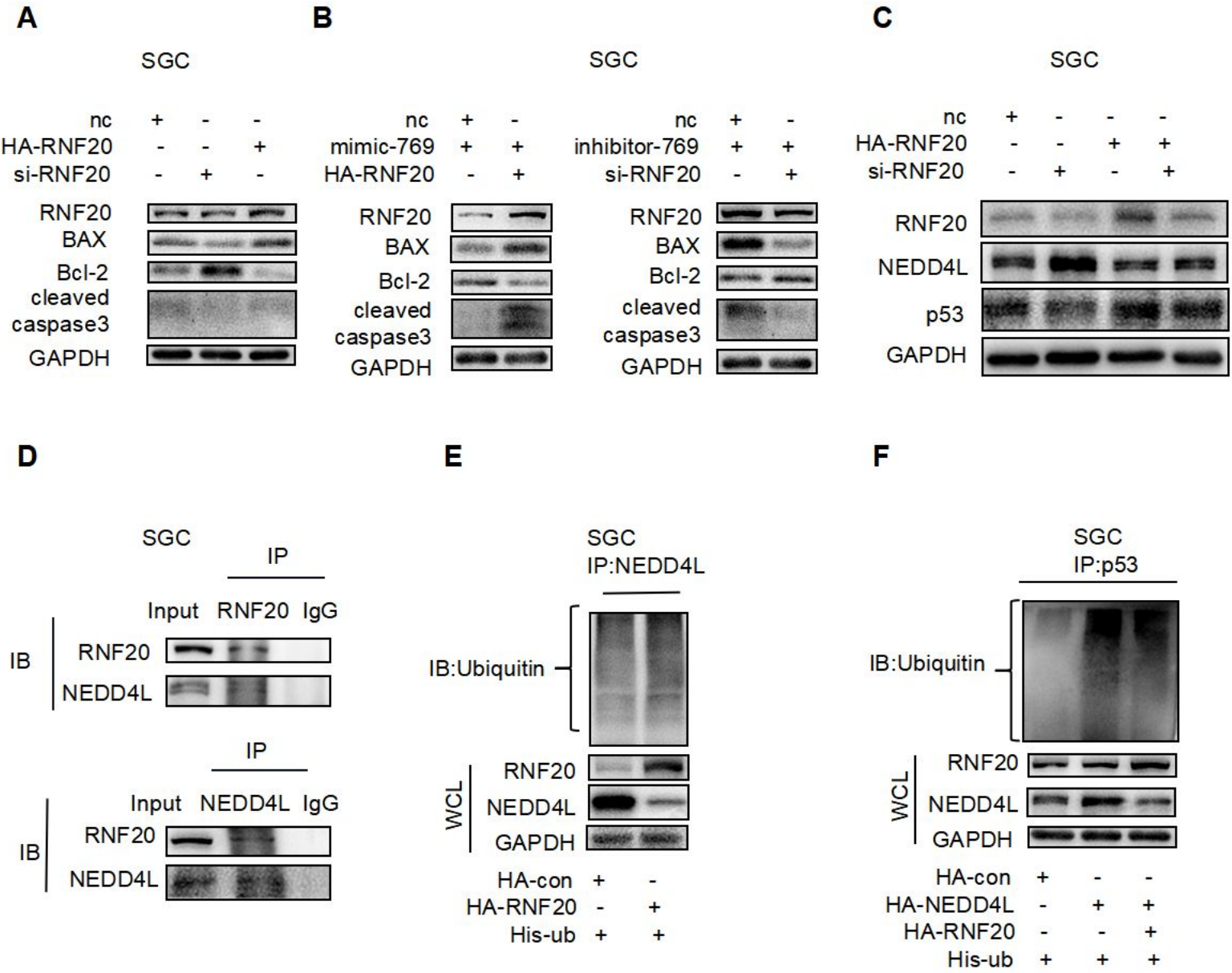
A
SGC
nc + - -
HA-RNF20 - - +
si-RNF20 - + -
RNF20
BAX
Bcl-2
cleaved caspase3
GAPDH
B
SGC
nc + -
mimic-769 + +
HA-RNF20 - +
RNF20
BAX
Bcl-2
cleaved caspase3
GAPDH
SGC
nc + -
inhibitor-769 + +
si-RNF20 - +
RNF20
BAX
Bcl-2
cleaved caspase3
GAPDH
C
SGC
nc + - - -
HA-RNF20 - - + +
si-RNF20 - + - +
RNF20
NEDD4L
p53
GAPDH
D
SGC
IP
Input RNF20 IgG
IB
RNF20
NEDD4L
IP
Input NEDD4L IgG
IB
RNF20
NEDD4L
E
SGC
IP:NEDD4L
IB:Ubiquitin
WCL
RNF20
NEDD4L
GAPDH
HA-con + -
HA-RNF20 - +
His-ub + +
F
SGC
IP:p53
IB:Ubiquitin
WCL
RNF20
NEDD4L
GAPDH
HA-con + - -
HA-NEDD4L - + +
HA-RNF20 - - +
His-ub + + +